INFLUENZA

An influenza H1 hemagglutinin stem-only immunogen elicits a broadly cross-reactive B cell response in humans

Sarah F. Andrews*, Lauren Y. Cominsky†, Geoffrey D. Shimberg†, Rebecca A. Gillespie†, Jason Gorman†, Julie E. Raab†, Joshua Brand, Adrian Creanga, Suprabhath R. Gajjala, Sandeep Narpala, Crystal S. F. Cheung, Darcy R. Harris, Tongqing Zhou, Ingelise Gordon, LaSonji Holman, Floreliz Mendoza, Katherine V. Houser, Grace L. Chen, John R. Mascola, Barney S. Graham, Peter D. Kwong, Alicia Widge, Lesia K. Dropulic, Julie E. Ledgerwood, Masaru Kanekiyo, Adrian B. McDermott

Current yearly seasonal influenza vaccines primarily induce an antibody response directed against the immunodominant but continually diversifying hemagglutinin (HA) head region. These antibody responses provide protection against the vaccinating strain but little cross-protection against other influenza strains or subtypes. To focus the immune response on subdominant but more conserved epitopes on the HA stem that might protect against a broad range of influenza strains, we developed a stabilized H1 stem immunogen lacking the immunodominant head displayed on a ferritin nanoparticle (H1ssF). Here, we evaluated the B cell response to H1ssF in healthy adults ages 18 to 70 in a phase 1 clinical trial (NCT03814720). We observed both a strong plasmablast response and sustained elicitation of cross-reactive HA stem–specific memory B cells after vaccination with H1ssF in individuals of all ages. The B cell response was focused on two conserved epitopes on the H1 stem, with a highly restricted immunoglobulin repertoire unique to each epitope. On average, two-thirds of the B cell and serological antibody response recognized a central epitope on the H1 stem and exhibited broad neutralization across group 1 influenza virus subtypes. The remaining third recognized an epitope near the viral membrane anchor and was largely limited to H1 strains. Together, we demonstrate that an H1 HA immunogen lacking the immunodominant HA head produces a robust and broadly neutralizing HA stem–directed B cell response.

INTRODUCTION

Influenza virus epidemics are typically associated with 290,000 to 650,000 deaths annually worldwide (*1*). In addition, H1N1, H3N2, and H2N2 influenza subtypes have caused pandemics in the past 100 years with increased mortality rates, including the 1918 H1N1 influenza pandemic, which was responsible for 20 million to 50 million deaths. The high mutability of influenza virus and existence of ample animal reservoirs make the emergence of another pandemic highly likely.

Hemagglutinin (HA) is the most abundant glycoprotein on the influenza virus surface. Within influenza type A, HA can be divided phylogenetically into 18 subtypes that segregate into two groups, group 1 and group 2. HA is composed of a head and stem domain. Protection against influenza infection correlates with titers of antibodies (Abs) that bind the receptor binding site in the HA head domain, blocking viral attachment and infection of cells. Seasonal influenza vaccines that are annually updated to include the current circulating influenza strains primarily induce an Ab response directed against the immunodominant, but continually diversifying, HA head region. These Ab responses provide influenza strain–specific protection but only limited cross-protection against other strains, even within the same subtype. For this reason, immunogens that elicit immune responses focused on subdominant but more conserved epitopes, such as those on the HA stem, are being developed (*2*). The expectation is that these immunogens would elicit broadly neutralizing responses that would protect against antigenically drifted or shifted influenza strains, including those with pandemic potential.

Responses to conserved HA stem–specific epitopes are prominent only in the absence of preexisting immunity to strain-specific HA head epitopes (*3*, *4*). Broadly protective Ab responses to HA stem–specific epitopes were first described in the 1990s (*5*, *6*) but were largely unappreciated until structural studies identified heterosubtypic neutralizing Abs directed to the HA stem (*7*, *8*) and until HA stem–specific responses were observed to dominate the early response to the 2009 H1N1 pandemic strain (*4*, *9*–*11*). Since then, several studies have shown that first exposure through infection or vaccination to new influenza subtypes such as H5N1, H2N2, H9N2, or H7N9 also induces a strong HA stem–specific B cell response (*12*–*17*). However, upon second exposure to these immunogens, responses to the strain-specific HA head epitopes begin to dominate, making them unsuitable for regular expansion of HA stem–specific immune responses (*13*, *14*, *18*–*20*). To overcome this HA head immunodominance, we developed an H1 stabilized stem trimer from the H1N1 A/NewCaledonia/20/1999 (NC99) HA that lacks the head domain (*21*). This construct was genetically fused to the ferritin subunit from *Helicobacter pylori* to produce multimeric H1 stabilized stem self-assembling nanoparticles (H1ssF) (*21*, *22*). Animal studies with this immunogen showed that it induced strong serological binding titers against diverse group 1 influenza subtypes and

Vaccine Research Center, National Institute of Allergy and Infectious Diseases, National Institutes of Health, Bethesda, MD 20902, USA.
†These authors contributed equally to this work.
*Corresponding author. Email: sarah.andrews2@nih.gov

conferred Ab-mediated protection against heterosubtypic H5N1 infection in mice and ferrets (*21*).

Here, we describe the human B cell response to H1ssF in a phase 1 clinical trial (NCT03814720) in healthy adults ages 18 to 70. We found that vaccination with this product generated a strong plasmablast response and sustained memory B cell response regardless of age. Investigation of the immunoglobulin (Ig) repertoire and Ab functionality of responding B cells indicated that they targeted two conserved epitopes on the H1 stem. The majority of the expanded B cells expressed Abs capable of broadly neutralizing virus strains across group 1 subtypes, including those of pandemic potential. Thus, vaccination with a stem-only HA immunogen elicits a strong B cell response targeting conserved HA epitopes that could provide broader protection against diverse influenza virus strains.

RESULTS

H1ssF nanoparticle vaccination elicited robust plasmablast responses

We investigated the B cell response to two doses of an H1 stabilized stem ferritin nanoparticle (H1ssF) vaccine in a phase 1 clinical trial with participants divided into five groups. Four groups, stratified by age, received two 60-μg vaccine doses 4 months apart, and one group received one 20-μg dose. A transitory burst of Ab-secreting plasmablasts is present in peripheral blood between days 5 and 7 after vaccination and represents the earliest B cells directly activated and differentiated by the immunogen. To characterize the plasmablast response, we isolated peripheral blood mononuclear cells (PBMCs) from fresh blood collected days 5 to 7 after the first H1ssF dose from 50 of the 52 participants enrolled in the study. We used fluorescently labeled H1 A/New Caledonia/20/1999 (NC99) ectodomain and matched stabilized stem soluble trimers to detect H1 stem–binding plasmablasts ($CD19^+$ $CD20^-$ $CD21^-$ $CD27^{hi}$ $CD38^{hi}$) (Fig. 1A and fig. S1A). We observed plasmablasts recognizing the H1 stabilized stem and ectodomain in 49 of 50 participants ranging from 56 to 54,000 H1 stem–specific plasmablasts per million $CD19^+$ B cells, with a mean of 6063 (Fig. 1B). In contrast, upon vaccination with the 2020–2021 seasonal quadrivalent influenza vaccine (QIV), a mean of 800 H1 stem–specific plasmablasts per million $CD19^+$ B cells recognized the H1 stem (Fig. 1B). On average, 29 and 2% of total plasmablasts were specific for the H1 stem after H1ssF and QIV immunization, respectively (fig. S1B). There was no difference detected in the number of H1 stem–specific plasmablasts between the 20- and 60-μg dose H1ssF groups or between the different age groups (Fig. 1C). In summary, we observed a robust H1 stem–specific plasmablast response in all age groups 1 week after the first H1ssF vaccine dose.

H1 stem–directed plasmablasts bind two distinct stem epitopes

In every participant, we observed two distinct populations of H1 stem–binding plasmablasts, with one population showing higher binding to the H1 stem (upper population, red) than the other (lower population, blue) (Fig. 1A). The proportion of H1 stem–binding plasmablasts in this lower population varied across participants from 3 to 83% with a mean of 30% (Fig. 1D and fig. S1B). To further understand these two H1 $stem^+$ populations, we bulk-sorted plasmablasts in the lower and upper populations, sorted H1 $stem^-$ plasmablasts into separate tubes, and did droplet-based single-cell RNA sequencing to amplify and sequence paired heavy chain (HC) and light chain (LC) Ig sequences from thousands of plasmablasts in each of three participants with high responses after immunization with 60 μg of H1ssF. We observed a restricted and distinct variable gene usage in the two H1 stem–binding plasmablast populations; the HA $stem^-$ plasmablasts had a very diverse Ig repertoire (Fig. 1E). More than 80% of the HA $stem^-$ plasmablasts were clonally distinct from the H1 stem–binding populations (fig. S1C). The mean variable heavy chain (VH) mutation frequency was equivalent between all populations (fig. S1D). Both the upper and lower H1 stem–binding plasmablast populations were primarily IgG, whereas the plasmablast H1 $stem^-$ population was largely IgA (fig. S1E), indicating that it likely represents baseline circulating plasmablasts of mucosal origin (*23*, *24*).

Various multidonor or public classes of Igs, defined as Igs with similar genetic characteristics and modes of recognition present in multiple individuals, have been identified that recognize the H1 stem (*25*, *26*). The upper H1 stem–binding population was dominated by the expression of Igs that match the extensively characterized VH1-69 HC paired with a kappa LC class that binds a central epitope on the HA stem at the $Trp21_{HA2}$ pocket (Fig. 1, E and F) (*7*, *27*, *28*). However, plasmablasts in the lower population largely expressed VH3-23 paired with either VK3-15 or VK3-11 (Fig. 1E, middle). One multidonor class that binds an epitope on the HA ectodomain just above the viral membrane anchor (hereafter referred to as anchor epitope) (Fig. 1F) was recently described as VH3-23, VH3-30/3, or VH3-48 paired with either VK3-11 and VK3-15 with a highly canonical 10–amino acid LC complementary determining region 3 (CDRL3) with a conserved NWP motif (referred to as VH3+NWP hereafter) (*29*). Eighty percent of all sequenced plasmablasts in the lower population matched this VH/VL criterion versus 0.1% of Ig sequences from plasmablasts in the upper population (Fig. 1G and fig. S1, F and G). Furthermore, we obtained a cryo–electron microscopy (cryo-EM) structure of one VH3+NWP monoclonal Ab (mAb) (204-1B06) isolated from a plasmablast in the lower population in complex with H1 NC99 HA (Fig. 1H and fig. S2, A to F). Structural analysis confirmed that 204-1B06 bound the H1 stem below the central epitope recognized by VH1-69 class mAb 310-1B11 (*16*) and overlapped with FISW84, a VH3+NWP mAb first described binding this anchor epitope (Fig. 1, I and J) (*30*).

On the basis of the dichotomous Ig repertoire we observed between the upper and lower populations, we assumed that the upper population represented the plasmablasts binding the central epitope on the HA stem, whereas the lower population consisted of plasmablasts binding the anchor epitope. To confirm this, we made an H1 NC99 HA with a glycan at residue 27_{HA2} (H1-N27) predicted to block binding to the anchor epitope by steric hindrance (Fig. 1K). We also had an HA with a glycan at 45_{HA2} (H1-N45) described previously to block binding to the central epitope (Fig. 1K) (*31*). In addition, we made an H1 NC99 HA with glycans at both 45_{HA2} and 27_{HA2} (H1-N45/27). As predicted, 204-1B06 and FISW84 showed no binding to H1-N27 but could bind H1-N45, whereas VH1-69 mAbs 310-1B11 and CR9114 (*32*) bound H1-N27, but not H1-N45 (Fig. 1L and fig. S3A). We then stained PBMCs from a participant 2 weeks after H1ssF vaccination with H1 wild type (H1-WT), H1-N27, H1-N45, or H1-N45/27 and saw that the upper and lower H1 stem–specific memory B cell populations segregated into H1-$N27^{pos}$ H1-$N45^{neg}$ and H1-$N27^{neg}$ H1-

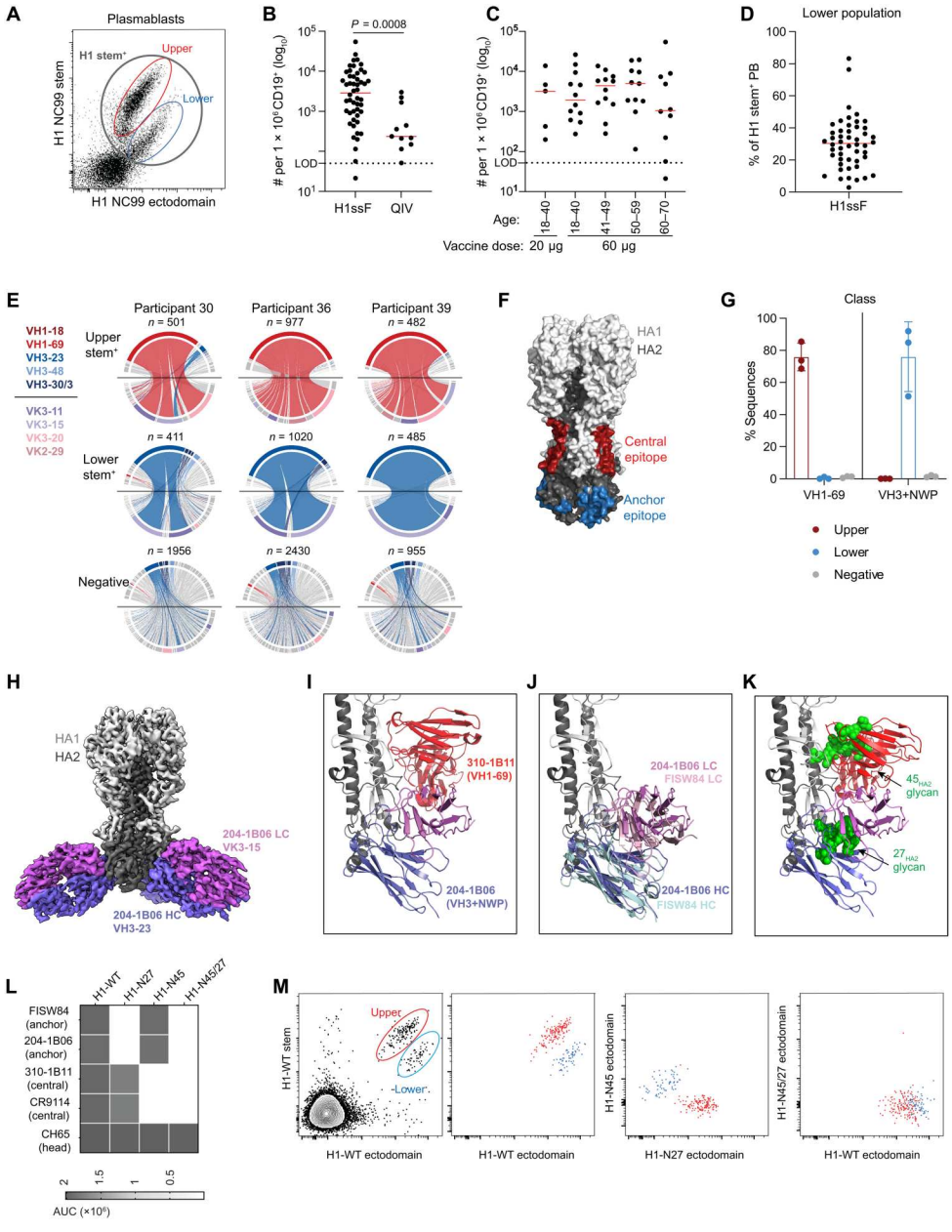

Fig. 1. Plasmablast response to H1ssF targets two H1 stem epitopes. (**A**) Flow cytometry plot showing CD19$^+$ CD20$^-$ CD27^{hi} CD38^{hi} plasmablasts binding to the H1 NC99 ectodomain and stem soluble trimers. The gray circle indicates all H1 stem–specific plasmablasts. Red and blue gates indicate the upper and lower H1 stem–binding plasmablast populations. (**B** and **C**) Number of H1 NC99 stem–specific plasmablasts per million CD19$^+$ B cells as indicated by the gray gate in (A) in all participants together (B) or divided by vaccine group (C). Each dot represents one participant ($n = 50$ for H1ssF and $n = 11$ for QIV), with mean indicated by the red lines. Statistical significance was determined by Mann-Whitney t test. LOD, limit of detection based on number of probe$^+$ plasmablasts in an unvaccinated individual. (**D**) Proportion of all H1 stem–binding plasmablasts (PB) in the lower population in each participant, with the mean indicated by the red line. (**E**) Chord diagrams showing variable heavy (VH) and variable light (VL) gene pairs for plasmablasts, with total number of sequence pairs indicated above each plot. The top half of the chord diagram has the VH genes linked to VL genes in the bottom half. The most abundant VH and VL genes are colored as indicated; all other Ig genes are shown in gray. Each link indicates a separate VH/VL chain gene pair combination. (**F**) Surface representation of HA, with HA1 in light gray and HA2 in dark gray. The central (red) and anchor (blue) epitopes are highlighted on the basis of 5 Å Fab footprints of 310-1B11 and FISW84, respectively. (**G**) Proportion of sequences from each plasmablast population that are either a VH1-69 class or VH3+NWP class. The mean with SD for the three donors in (E) is shown. (**H**) Cryo-EM density is shown for binding of 204-1B06 Fab (blue and purple) with the NC99 H1 HA trimer. (**I** and **J**) Ribbon diagrams show the H1 NC99 stem region with binding of 204-1B06 Fab and 310-1B11 Fab (PDB ID: 7LOL) (I) or FISW84 Fab (PDB ID: 6HJP) (J). (**K**) Ribbon diagram showing model Man5 glycans at 27_{HA2} and 45_{HA2}, with 310-1B11 and 204-1B06 Fab binding the H1 stem. The 27_{HA2} glycan disrupts an H-bond between 27_{HA2} and Arg100c$_{HC}$ as well as clashing with other 204-1B06 HC and LC interactions. The 45_{HA2} glycan replaces a hydrophobic residue commonly targeted by VH1-69 Abs and sterically blocks the core of the central epitope. (**L**) Binding area under the curve (AUC) of indicated mAbs against H1-WT, H1-N27, H1-N45, and H1-N27/45 ectodomains. (**M**) Flow cytometry plots of CD19$^+$ CD20$^+$ IgG$^+$ memory B cells stained with H1-WT stem and H1-WT, H1-N27, H1-N45, and H1-N27/45 ectodomains. Cells circled in the red and blue gates in the first panel were overlaid and colored to match the circles for panels 2 to 4. Two-dimensional flow plots of cells in the two populations binding the indicated proteins are shown.

N45^{pos} populations, respectively (Fig. 1M). Cells able to bind the H1 stem with glycans at both positions (H1-N45/27) were virtually undetectable (Fig. 1M). We further sorted and sequenced the H1 stem–specific memory B cells from two participants and found that 98% of H1-N27^{neg} H1-N45^{pos} memory B cells expressed Igs with a VH3+NWP signature (fig. S3B). Sixty-three percent of the H1-N45^{neg} H1-N27^{pos} memory B cells belonged to the VH1-69 class, whereas 0.1% had a VH3+NWP signature (fig. S3B). Together, we conclude that the plasmablast response after H1ssF vaccination recognizes two regions on the H1 stem that can be distinguished on the basis of differential binding by flow cytometry to H1 ectodomain and stabilized stem soluble trimers.

The Ig repertoire of the plasmablast response is highly restricted across participants

To characterize the Ig repertoire of plasmablasts in a larger group of participants, we single cell–sorted H1 stem–specific plasmablasts from 20 individuals (including the same 3 we bulk-sorted above) across vaccine groups and amplified paired HC and LC from each cell, obtaining 40 to 130 paired sequences per participant. The

single cell–sorted and bulk-sorted Ig sequencing from the three participants yielded very similar results by both methodologies (see Fig. 1E and fig. S4A). By index sorting, we were able to determine which Ig sequences came from single cell–sorted plasmablasts in the upper or lower H1 stem–binding populations. Cells in the upper population binding the central epitope were dominated by the VH1-69 class, representing greater than 45% of all Ig HC sequences in that population in 19 of 20 participants (Fig. 2, A and B, and fig. S4, B to D). The one participant with a low frequency of the VH1-69 class had instead a large clonal expansion of the previously described cross-group VH6-1 multidonor class (Fig. 2A, bottom right pie chart) (*33*, *34*). The previously identified VH1-8+ILTG multidonor class (*33*) was also detected in a subset of participants at low frequencies (Fig. 2, A and B). In the lower population, 80% of the plasmablast sequences matched the anchor epitope–binding VH3+NWP class (Fig. 2B). We detected at least one sequence belonging to this class in all but the participant with the VH6-1 clone (Fig. 2, A and B). Overall, 80% of the H1 stem–binding plasmablasts expressed an Ig matching a previously described multidonor class, with 50% on average belonging to the VH1-69 class and 23% belonging to the VH3+NWP class (Fig. 2C). Within each of these classes, we detected multiple distinct lineages within the same individual, indicating that it was a polyclonal response but with highly biased VH/VL usage (Fig. 2A). We observed no difference in class usage between those who received a low or high dose of the vaccine (fig. S4E). We conclude that the plasmablast response to the H1ssF vaccine targeted two major epitopes on the H1 stem dominated by two multidonor classes.

One-third of serum Abs bind the anchor epitope

Because plasmablasts are actively secreting Abs, we wanted to look at the relative contribution of Abs binding to the two epitopes in the serum after H1ssF vaccination. We used two different methods to measure the fraction of serum Abs binding the anchor epitope in 12 participants 2 weeks after the first H1ssF dose. For this analysis, we chose three participants from each age group that received the 60-μg dose with varying amounts of plasmablasts targeting the anchor epitope. First, we depleted Abs binding different H1 stem epitopes by incubating the serum samples with magnetic beads coated with H1-WT, H1-N27, or no HA. The relative abundance of the remaining H1 stem–specific serum Abs after depleting out Abs binding each of these HAs was then measured. Second, we measured the concentration of serum Abs binding H1 NC99 stem in the presence or absence of 310-1B11 Fab that binds and blocks the central epitope, leaving primarily anchor epitope–binding serum Abs. Control experiments with mAbs verified that both assays worked as expected (fig. S5, A and B). We saw a decrease, but not complete absence, of H1 stem binding after depleting central epitope–binding Abs with H1-N27 or by blocking this epitope with 310-1B11 Fab, thus leaving serum Abs binding the anchor epitope (Fig. 3, A and B). The fraction of H1 stem–binding serum Abs binding the anchor epitope relative to total serum H1 stem binding in both assays correlated well with each other (Fig. 3C). The fraction of serum Abs

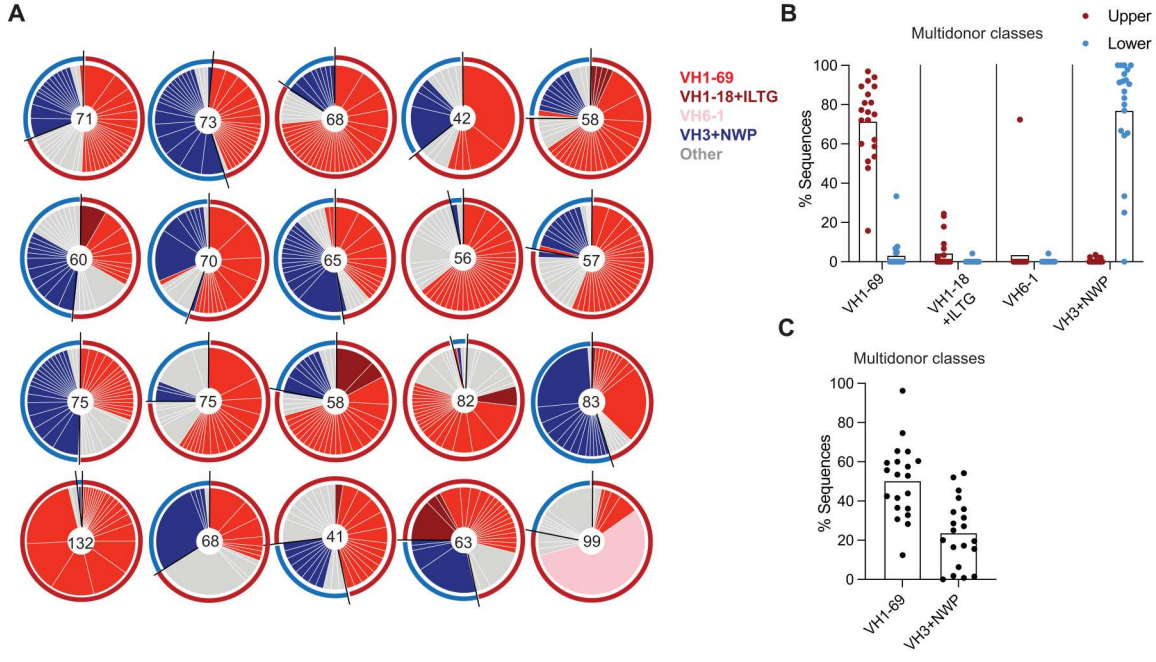

Fig. 2. Multidonor Ig classes dominate the plasmablast response. (**A**) Pie charts of VH sequences from all H1 stem–binding plasmablasts. Each pie chart represents sequence data from one participant, with the number in the center indicating the total number of sequences for that participant. Each pie slice indicates a separate clonal lineage. Lineages belonging to the VH1-69, VH18+ILTG, VH6-1, and VH3+NWP classes are color-coded as indicated. Lineages not matching any of these classes are in gray. Red arcs around the outside of the pie chart indicate sequences from plasmablasts from the upper H1 stem–binding population, and blue arcs indicate sequences from plasmablasts in the lower H1 stem–binding population. The first three pie charts are the same participants as shown in Fig. 1E. (**B**) Proportion of sequences from single cell–sorted plasmablasts in the H1 stem upper or lower populations belonging to each of the indicated multidonor classes. Each dot represents one participant, with the bar indicating the mean. (**C**) Proportion of all H1 stem–binding plasmablasts expressing Igs belonging to the VH1-69 or VH3+NWP class. Each dot represents one participant, with the bar indicating the mean. n = 20 participants for (A) to (C).

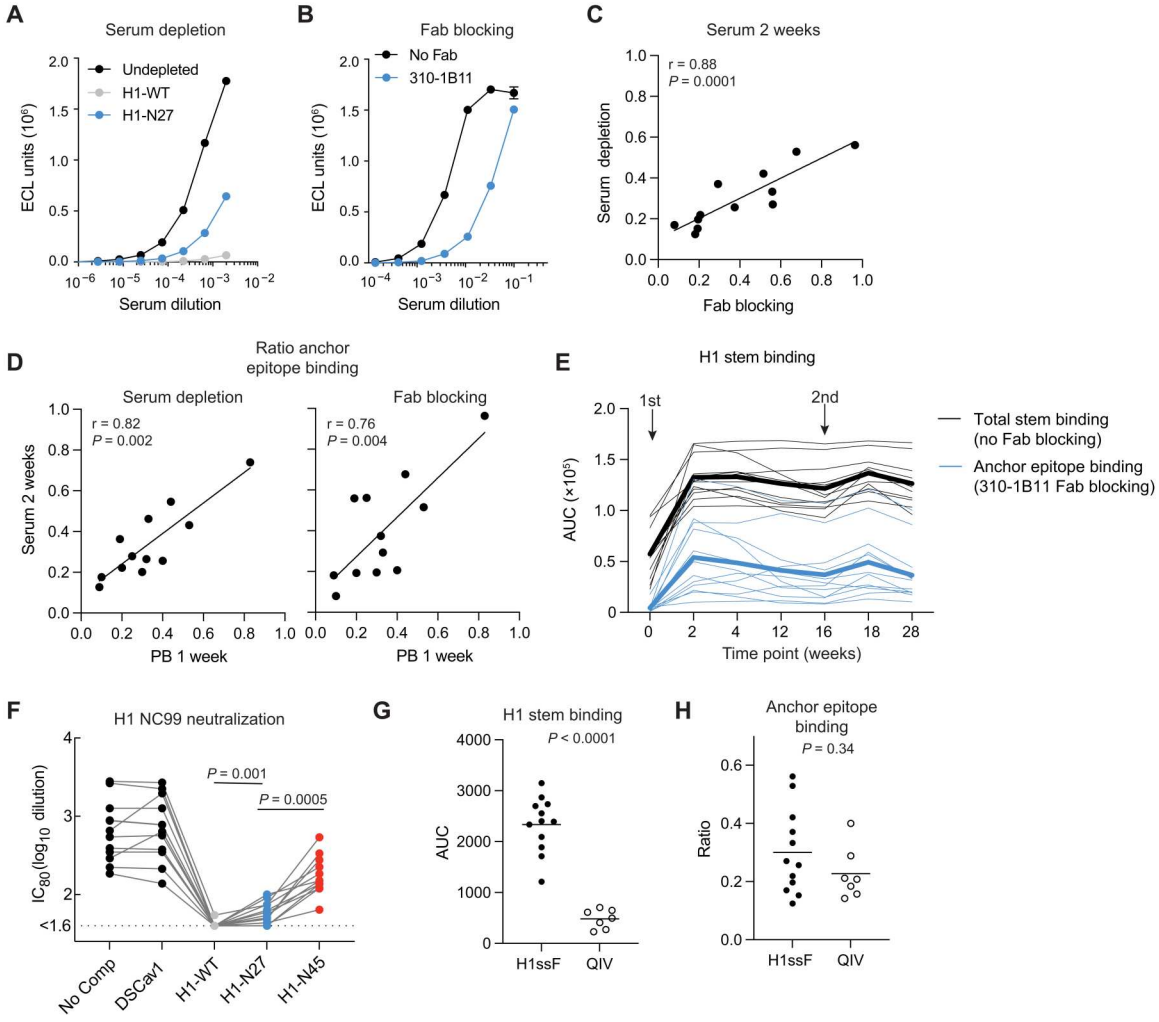

Fig. 3. A third of serum antibodies bind the anchor epitope. (**A**) Representative binding plot of serum samples collected 2 weeks after the first H1ssF dose to H1 stem after preincubation with magnetic beads coated with no HA (undepleted), beads coated with H1-WT to bind and remove all H1-specific Abs, or beads coated with H1-N27 to bind and remove all Abs except those that bind the anchor epitope blocked by N27. ECL, electrochemiluminescence. (**B**) Representative binding plot of the same serum sample as in (A) tested for binding to H1 stem without blocking (no Fab) or in the presence of an antibody Fab (310-1B11) that blocks all binding to the central stem epitope so that only binding to the anchor epitope is detected. (**C**) Correlation between the ratio of serum Abs binding the anchor epitope compared with all H1 stem binding as detected by the serum depletion and Fab blocking experiment. (**D**) Correlation between the proportion of H1 stem–binding plasmablasts at 1 week after the first H1ssF dose binding the anchor epitope and the ratio of serum Abs at 2 weeks binding to the same epitope as detected by the serum depletion method (left) or the Fab blocking method (right). For (C) and (D), each dot represents one participant with linear regression line. The Pearson correlation *r* value and *P* value are indicated. (**E**) Binding AUC to H1 NC99 stem of serum samples across seven time points either with or without addition of the 310-1B11 Fab to detect all H1 stem binding (in black) or only Abs binding the anchor epitope (in blue). Thin lines indicate data from each participant, with thick lines indicating the mean. All serum depletion and Fab competition studies are representative of one or two independent experiments, depending on the participant. (**F**) The capacity to neutralize H1N1 NC99 virus was tested with serum samples collected at 2 weeks after the first H1ssF dose in the absence or presence of competing HAs as indicated. DSCav1, an RSV spike protein, was used as a noncompeting control. The $\log_{10}$ 80% inhibitory serum dilution (IC_{80}) is shown, with lines connecting the same serum samples tested with different competing antigens. Statistical significance was determined by Wilcoxon matched pairs *t* test. Representative data of two independent experiments are shown. (**G** and **H**) Binding AUC to H1-WT stem (G) or ratio of serum Abs binding the anchor stem epitope compared with total H1 stem–binding Abs as detected by the serum depletion assay (H) for serum samples collected at 2 weeks after one dose of the H1ssF vaccine or the 2020–2021 QIV as indicated. Each dot represents data from one participant, and the lines indicate mean values. $n = 12$ for H1ssF for (A) to (H) and $n = 7$ for QIV. Statistical significance for (G) and (H) was determined by Mann-Whitney *t* test.

binding the anchor epitope at 2 weeks after the first H1ssF dose also correlated with the fraction of plasmablasts binding this epitope at week 1 for each participant (Fig. 3D). We further measured the fraction of anchor epitope binding in serum samples at multiple time points with the Fab blocking method. Serum Abs binding the anchor epitope were virtually undetectable before vaccination but increased by 2 weeks after the first H1ssF dose and remained elevated with a similar kinetic as total H1 stem–binding Abs through week 28 (Fig. 3E and fig. S5C). Thus, the fraction of serum Abs binding the anchor epitope after H1ssF vaccination approximated the fraction of plasmablasts binding this epitope and remained elevated up to 7 months after receiving two doses of the H1ssF vaccine.

To determine the contribution of Abs binding the central and anchor stem epitopes to serum neutralization of H1N1 NC99 influenza virus, we did a competition microneutralization assay with H1-WT, H1-N27, H1-N45 HAs, and a control respiratory syncytial virus (RSV) protein, DSCav1, 2 weeks after the first H1ssF vaccine. Addition of these HAs inhibited the neutralization of control mAbs as expected (fig. S5D). H1-WT blocked all serum neutralization of NC99 virus, whereas we saw a partial reduction in serum neutralization with H1-N45, which blocks all but central stem epitope–binding Abs (Fig. 3F). Serum competed with H1-N27, in which all but anchor epitope–binding serum Abs are blocked, had a more substantially reduced neutralization titer against H1 NC99 virus (Fig. 3F).

We also tested serum samples from seven participants with a detectable H1 stem plasmablast response 2 weeks after the 2020–2021 QIV for the presence of anchor epitope stem–binding Abs using the serum depletion assay. We observed much lower concentrations of H1 stem–binding Abs in serum samples from QIV-vaccinated individuals (Fig. 3G) but detected no difference in the fraction binding the anchor epitope between QIV and H1ssF vaccination (Fig. 3H and fig. S5E). Thus, Abs binding the H1 anchor stem epitope represent, on average, about one-third of all H1 stem–binding serum Abs 2 weeks after H1ssF or QIV vaccination.

Sustained H1 stem–specific memory B cell response recognizing both stem epitopes

We next looked at the memory B cell response to H1ssF by measuring the frequency of $CD19^+$ $CD20^+$ B cells that bound both the H1 NC99 ectodomain and stabilized stem by flow cytometry (fig. S6, A and B). Staining the cells with a fluorescently labeled stabilized stem ferritin nanoparticle instead of soluble stem trimers had a very similar binding profile (fig. S6C). We measured the H1ssF-specific response from the day of the first H1ssF dose through 12 weeks after receiving the second H1ssF dose in all 23 participants from the four age groups that received the 60-μg doses from whom PBMCs were collected at all time points. We observed an increase in IgG and IgA H1 stem–specific memory B cells after the first H1ssF dose and a smaller increase in IgG H1 stem–specific memory B cells after the second H1ssF dose (Fig. 4A). On average, we observed a 16-fold increase in the proportion of isotype switched H1 stem–specific memory B cells at 2 weeks after the first H1ssF dose and a roughly 4.5-fold increase after the second dose (Fig. 4, A and B). H1 stem–specific memory B cells remained about 2.5-fold higher 12 weeks after the second H1ssF dose compared with prevaccination frequencies (P = 0.0001, Wilcoxon matched pairs test) (Fig. 4, A and B). We detected no difference in the magnitude of the H1 stem–specific memory B cell response between age groups at the peak time point after the first dose (fig. S7, A and B). No change in the proportion of H1 head–binding memory B cells (H1 ectodomain$^+$ H1 stem−) was observed upon vaccination with H1ssF (fig. S7C).

Like the plasmablasts, we were able to detect memory B cells binding to the central and anchor H1 stem epitopes on the basis of differential binding to the H1 NC99 ectodomain and stabilized stem (fig. S6, A and B). Similar to the plasmablast response, an average of about 30% of the H1 stem–specific memory B cells recognized the anchor epitope, with the remaining binding the central epitope at week 2 after H1ssF vaccination (Fig. 4C). The proportion of plasmablasts and memory B cells binding to each epitope correlated for each participant (fig. S7D). The ratio of memory B cells binding the anchor epitope was also similar before and after vaccination, indicating proportional boosting of preexisting memory B cells binding the two epitopes by the H1ssF vaccine (Fig. 4C). In addition, we detected no difference in percent VH somatic hypermutation among H1 stem–specific lineages after the first and second vaccine doses, indicating little evolution of the H1 stem–specific memory B cell repertoire between the two doses (fig. S7, E and F).

H1ssF immunization elicits higher H1 stem–specific memory response than QIV immunization

To compare the H1 stem memory B cell response elicited by the H1ssF vaccine and 2020–2021 QIV, we analyzed the H1 stem–specific memory B cell response in eight participants for whom PBMCs were available starting the day of receiving the 2020–2021 QIV through 16 weeks later (fig. S6B). We observed an increase in both H1 HA head– and H1 HA stem–specific isotype switched memory B cells after QIV vaccination, but the elicitation of H1 stem–specific memory B cells by QIV was significantly (P = 0.008) lower than in response to H1ssF vaccination when compared with the 19 age-matched individuals with equivalent time points in the H1ssF study (Fig. 4, D and E). The H1 stem–specific memory B cell response after the first H1ssF dose approximated the H1 head–specific response after QIV in magnitude (Fig. 4, D and E). However, when we looked at the proportion of H1 stem–binding B cells binding the central and anchor epitopes, we saw no difference in the ratio of memory B cells binding these two epitopes whether the participant was vaccinated with one dose of H1ssF or QIV (Fig. 4F).

To determine whether the Ig repertoire of H1 stem–specific memory B cells elicited by H1ssF or QIV was equivalent, we single-sorted IgG^+ H1 stem–specific B cells (fig. S6B) from 12 individuals 2 weeks after receiving either the first H1ssF dose or QIV selected on the basis of sample availability. We detected no difference in the overall VH repertoire, VL repertoire, degree of VH somatic hypermutation, or clonality of the H1 stem–specific memory B cells elicited by either trial (Fig. 4G and fig. S7, G to I). The proportion of H1 stem–specific memory B cells expressing Igs belonging to the VH1-69 or VH3+NWP multidonor classes was also not different between the two vaccine groups, though it varied from participant to participant (Fig. 4H). Thus, the H1ssF vaccine induces a larger boost in H1 stem–specific memory B cells than QIV, but the expanded memory B cells appear qualitatively similar, engaging the same epitopes and expressing Igs with comparable repertoires.

The central epitope–targeting Ab response is more broadly neutralizing than the anchor epitope–targeting Ab response

To determine the functional characteristics of H1 stem–specific B cells elicited by the H1ssF vaccine, we first looked at cross-reactivity to H2 and H5 by flow cytometry at 2 weeks after the first vaccination (fig. S6B). In both H1ssF- and QIV-vaccinated participants, we found that, on average, more than 80% of central epitope–binding B cells cross-reacted with H5 or H2 HA, and about 40% could bind H1, H5, and H2 (Fig. 5A and fig. S8A). On the other hand, about 10% of the anchor epitope–binding B cells could bind all three subtypes, and about 60% recognized H1 only (Fig. 5A and fig. S8A).

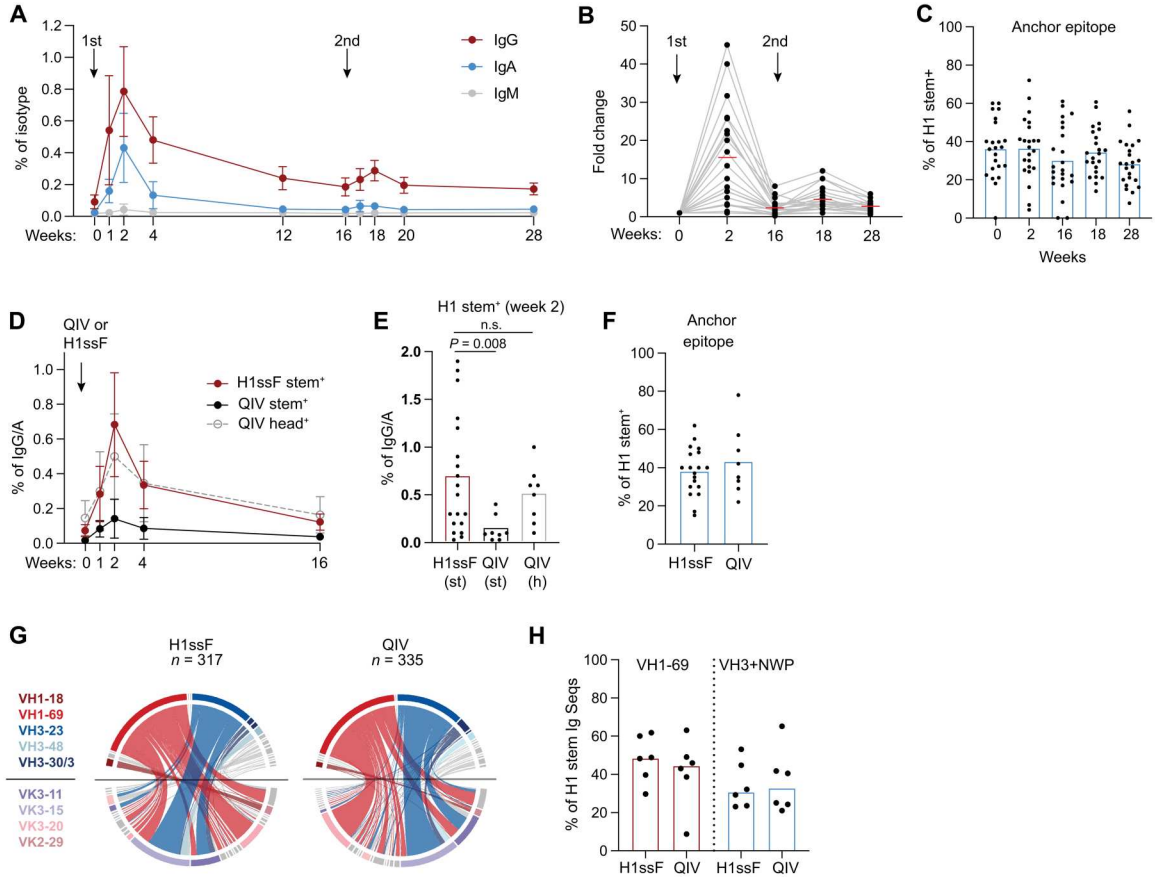

Fig. 4. H1ssF elicits a higher H1 stem–specific memory response than QIV. (**A** and **B**) PBMCs were stained with Abs to surface markers to identify memory B cells and fluorescently labeled H1 NC99 ectodomain and H1 NC99 stabilized stem as shown in fig. S6A. The proportion of $CD19^+$ $CD20^+$ IgG^+, IgA^+, or IgM $CD27^+$ memory B cells that recognized the H1 NC99 ectodomain and stabilized stem at different time points after the first and second dose of the H1ssF vaccine is shown. In (A), the mean ± 95% confidence interval (CI) is shown. In (B), the fold change from prevaccination to subsequent time points for all IgG or IgA (IgG/A) memory B cells is shown. Red lines in (B) indicate mean values. Each dot represents one participant connected across time points. (**C**) The proportion of H1 $stem^+$ memory IgG/A B cells that bound the anchor epitope was determined by flow cytometry as shown in fig. S6B at the indicated time points. Each dot represents one participant, with the bar indicating the mean at each time point. For (A) to (C), $n = 23$ individuals. (**D**) Mean ± 95% CI of the proportion of IgG/A memory B cells that bound the H1 NC99 ectodomain and H1 NC99 stabilized stem after H1ssF vaccination (H1ssF $stem^+$) or the H1 Hawaii/70/19 ectodomain (matching H1 strain in 2020–2021 QIV) and H1 Michigan/15 stabilized stem (QIV $stem^+$) or H1 Hawaii/70/19 ectodomain alone (QIV $head^+$) after QIV vaccination. (**E**) Same data at week 2 after vaccination as in (D), with each dot representing the data from one individual and the bar indicating the mean. st, stem; h, head. (**F**) Proportion of H1 $stem^+$ IgG/A memory B cells that bound the anchor epitope was determined by flow cytometry at 2 weeks after vaccination with H1ssF or QIV. The bars indicate the mean. For (D) to (F), $n = 8$ participants vaccinated with QIV and $n = 19$ participants vaccinated with H1ssF. All participants were ages 18 to 50. (**G** and **H**) H1 stem–specific B cells were single cell–sorted from IgG^+ memory B cells at 2 weeks after either QIV ($n = 6$ participants) or the first dose of the H1ssF ($n = 6$ participants), and paired Ig heavy and light chain were amplified and sequenced from each cell. (G) The VH/VL gene pairs are shown for all H1 stem–specific B cells isolated after either H1ssF or QIV vaccination as shown with the most abundant genes color-coded as in Fig. 2. (H) Proportion of sorted and sequenced H1 $stem^+$ B cells whose Ig belongs to either VH1-69 or VH3+NWP class. Each dot represents the proportion in one participant, with the bar indicating the mean. Seqs, sequences. Statistical significance for (E), (F), and (H) was determined using unpaired Mann-Whitney *t* test. n.s., not significant.

This indicated substantial differences in cross-reactivity between B cells recognizing the central and anchor epitopes. To characterize this further, we produced mAbs from 27 VH1-69 and 38 VH3+NWP class Igs expressed by H1 stem–specific B cells isolated from 24 participants who received H1ssF or QIV and tested their cross-reactivity and cross-neutralization to H2, H5, H6, and H9 group 1 subtypes. As expected, all VH1-69 class mAbs recognized H1-N27 but not H1-N45; the VH3+NWP class mAbs had opposite specificity (fig. S8B). Similar to what we observed by flow cytometry, we found that all mAbs recognizing the anchor epitope, whether elicited by H1ssF or QIV, could bind and neutralize pre- and post-2009 pandemic H1N1 strains A/NewCaledonia/20/99 (NC99) and A/Michigan/45/2015 (MI15); only about 30% recognized H5, and less than 10% bound H2, H6, or H9 (Fig. 5, B and C, and fig. S8B). On the other hand, more than 80% of VH1-69 class Abs cross-reacted with H5, H6, and H9, and more than 50% also recognized H2 (Fig. 5, B and C, and fig. S8B). mAbs binding the central epitope that were not VH1-69 class were also broadly cross-reactive to group 1 subtypes (fig. S8B).

We next compared binding affinity by biolayer interferometry against H1 NC99 and H1 MI15 virus for 15 central epitope and 17 anchor epitope mAbs belonging to the VH1-69 and

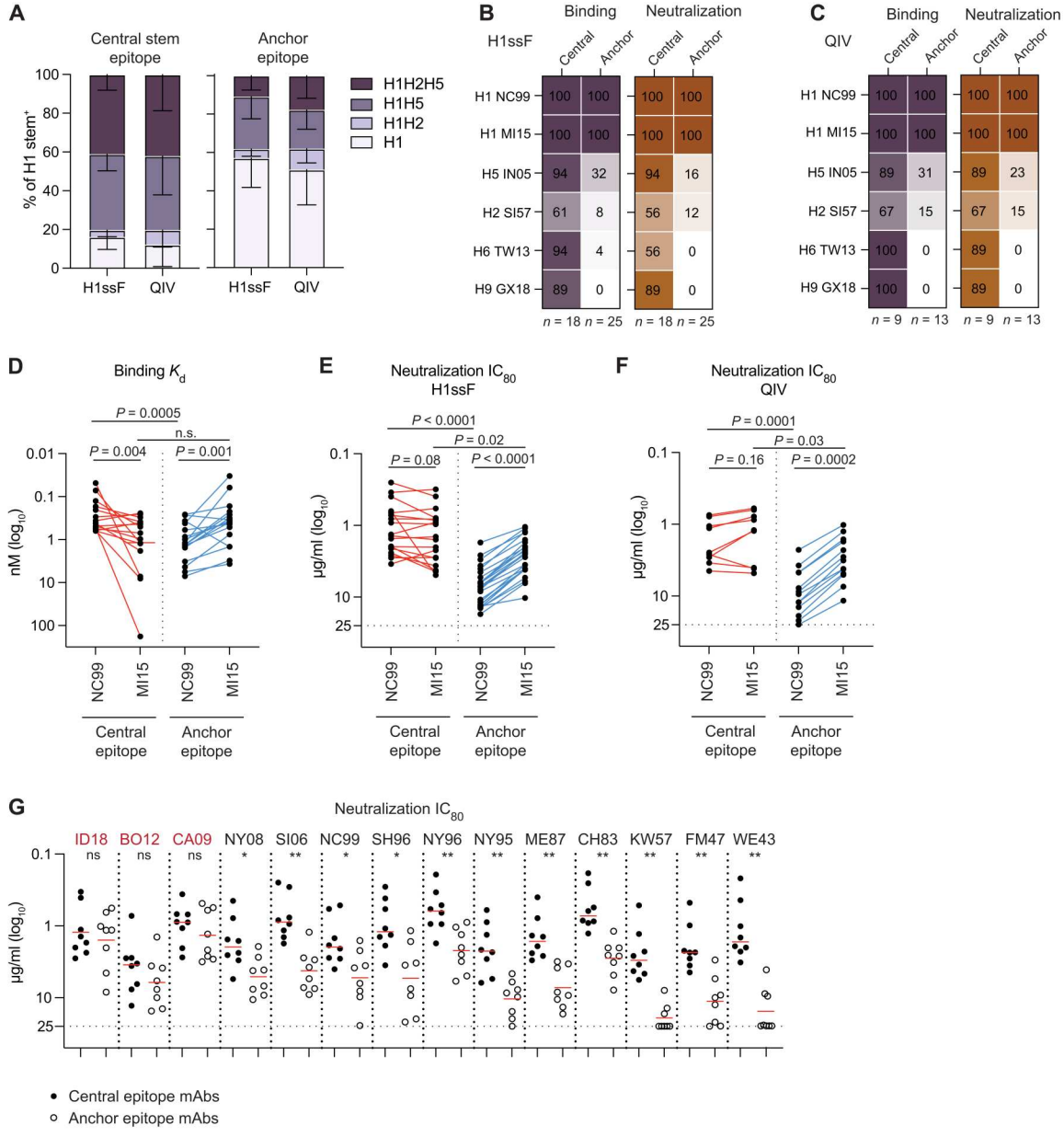

Fig. 5. Antibody responses targeting the central epitope are more broadly neutralizing. (**A**) IgG/A memory H1 stem–specific B cells binding to the central or anchor epitope were analyzed for binding to an H5 stabilized stem or H2 ectodomain by flow cytometry to determine cross-reactivity to these subtypes at 2 weeks after vaccination with QIV ($n = 8$) or H1ssF ($n = 13$). Mean and SD of the proportion of H1 stem–reactive B cells for each epitope with the indicated degree of cross-reactivity. (**B** and **C**) mAbs binding to the central epitope or anchor epitope were tested for binding to recombinant HA or the ability to neutralize virus in a microneutralization assay for various strains as indicated. Full virus strain names are in Materials and Methods. The percentage of mAbs able to bind HA (left, in purple) or neutralize virus (right, in orange) for each influenza strain is shown. The number of mAbs tested is indicated below. mAbs with an AUC above 4×10^5 are considered binding. mAbs with the capacity to inhibit viral growth of a given strain by 50% or more at 10 μg/ml are considered neutralizing. Data are shown for mAbs belonging to either the VH1-69 or VH3+NWP class isolated from memory B cells expanded after H1ssF vaccination (B) or QIV (C). (**D**) Fabs from a subset of mAbs from (B) were tested for binding to recombinant HA by biolayer interferometry. A comparison of the binding equilibrium constant (K_d) of Fabs to H1 NC99 and MI15 is shown. (**E** and **F**) Serial dilutions of all mAbs shown in (B) and (C) were tested for the capacity to neutralize NC99 or MI15 virus in a microneutralization assay. The $\log_{10}$ IC_{80} concentration for each mAb against H1N1 strains NC99 and MI15 is shown. Each dot indicates the IC_{80} for one mAb from samples from individuals vaccinated with H1ssF (E) or QIV (F). Lines in (D) to (F) connect data for each Ab for the two H1N1 strains. Affinity and neutralization data are representative of one or two independent experiments. The dotted horizontal lines in (E) and (F) indicate the lower limit of detection for the neutralization assay. (**G**) A subset of mAbs from (E) ($n = 8$ for each epitope) was tested for the capacity to neutralize a larger panel of H1N1 virus strains using the same assay. A side-by-side comparison of the IC_{80} of each mAb against the indicated virus recognizing either the central (closed circles) or anchor (open circles) HA stem epitope is shown. Virus strain names in red are post-2009 H1N1 pandemic strains. Red lines indicate the mean. The dotted horizontal line indicates lower limit of detection for the neutralization assay. Data are from one experiment with samples run in quadruplet. Statistical significance was determined by unpaired Mann-Whitney *t* test or paired Wilcoxon *t* test for (D) to (G). $^*P \leq 0.02$ and $^{**}P \leq 0.001$.

VH3+NWP class, respectively. mAbs binding the central epitope showed somewhat higher affinity to NC99, but mAbs binding the anchor epitope had lower affinity to NC99 compared with MI15 (Fig. 5D). When we compared neutralization potency to NC99 and MI15 virus, central epitope mAbs had equivalent neutralization potency to the two viruses, but anchor epitope mAbs had lower neutralization potency to NC99, mirroring the lower binding affinity to this H1N1 strain (Fig. 5E). mAbs isolated from B cells expanded after QIV showed this same pattern (Fig. 5F). We further tested neutralization with a subset of these mAbs isolated after H1ssF vaccination to 14 antigenically different H1N1 strains spanning from 1943 to 2018. mAbs binding the central and anchor epitopes showed equivalent neutralization potency to the three pandemic H1N1 strains, but anchor epitope–binding mAbs had substantially lower neutralization potency for all 11 H1N1 strains circulating before the 2009 H1N1 pandemic (Fig. 5G). Overall, we conclude that mAbs binding the central epitope, whether elicited by H1ssF or QIV, are more broadly neutralizing across group 1 subtypes than those binding the anchor epitope region. In addition, central epitope–binding mAbs had higher neutralization potency to more antigenically distant H1N1 strains.

Anchor epitope–specific B cells elicited by H5 or H2 vaccination are more cross-reactive than those elicited by H1 vaccination

Given the limited cross-reactivity to H2 and H5 of anchor epitope–binding B cells expanded by H1 vaccination, we wondered whether they were elicited with equal frequency upon immunization with H5 or H2. To evaluate this, we compared the proportion of H2H1 or H5H1 stem–reactive IgG memory B cells that bound the anchor epitope 2 weeks after the second dose of H1ssF, H2 ferritin nanoparticle (H2-F), or H5 monovalent inactivated (MIV) vaccines by flow cytometry (*19*, *35*). H2 circulated in the human population between 1957 and 1968, so we limited analysis to individuals born after 1970 who were thus naïve to both H2 and H5 before receiving the H2-F or H5 MIV vaccines (Fig. 6A). All available samples from participants that fit this age criterion from the three trials were analyzed. We found that the percentage of total H1 stem–binding memory B cells was not statistically different between the vaccine groups (Fig. 6B). However, a significantly higher proportion of the IgG HA stem–specific memory B cells recognized the anchor epitope after H1ssF vaccination compared with vaccination with an H5 ($P = 0.02$) or H2 ($P = 0.0002$) antigen, with H2-F vaccination eliciting the lowest proportion of anchor epitope–binding B cells (Fig. 6C). When we compared the Ig VH repertoire of HA stem–specific IgG memory B cells after each vaccine, we also saw decreasing amounts of the VH3+NWP class from H1ssF to H5 MIV to H2-F (Fig. 6D). However, both central epitope–binding and anchor epitope–binding H1 stem–specific memory B cells expanded after H5 MIV and H2-F vaccination were more cross-reactive by flow cytometry (Fig. 6E and fig. S9A). We expressed a few of the VH3+NWP mAbs detected in H5 MIV– and H2-F–vaccinated individuals and verified that they had enhanced cross-reactivity to H2 and H5, as we had seen by flow cytometry, but remained largely unable to bind or neutralize group 1 subtypes H6 and H9 (Fig. 6F and fig. S9B). In summary, the memory B cell response to H2 and H5 antigens is more cross-reactive and preferentially targets the central epitope compared with vaccination with H1.

Given the lower elicitation of anchor epitope–binding memory B cells after H2-F vaccination, we wondered whether individuals born before 1968 and first exposed to an H2 group 1 influenza strain had a lower abundance of anchor epitope–binding B cells in their memory B cell repertoire. In support of this hypothesis, there was a reduction in the proportion of stem binding memory B cells recognizing the anchor epitope after the first H1ssF dose in many vaccine participants born before 1965 (Fig. 6G). We also observed increased cross-reactivity of anchor and central epitope–binding memory B cells in individuals born before 1965 (Fig. 6H and fig. S9C). Thus, HA stem–reactive memory B cells elicited by the H1ssF vaccine in individuals born when H2, rather than H1, circulated in the human population preferentially target the central epitope and have increased cross-reactivity.

DISCUSSION

The discovery that broadly neutralizing Abs bind conserved sites on the HA stem has led to several efforts to develop immunogens that specifically elicit a B cell response directed toward these epitopes. In animal models, HA stem–specific Abs are protective against lethal challenges with seasonal and pandemic influenza strains, including H5N1 and H7N9 (*15*, *36*). HA stem–specific Abs induced by natural exposure or vaccination are unlikely to give full protection to influenza infection in humans alone. However, higher serum Ab concentrations have been associated with protection against infection and disease (*37*, *38*) and less probability of lower respiratory symptoms (*39*) in human cohort studies. Higher serum Ab concentrations also correlated with reduced shedding in a human influenza challenge study (*40*). Thus, broadly neutralizing HA stem–specific Abs could prove to be important, especially in the context of an influenza pandemic with an antigenically shifted strain where little preexisting immunity to HA head epitopes is present in the population.

Efforts to focus the immune response on conserved HA stem epitopes have included polypeptides mimicking the HA stem (*41*, *42*), headless HAs (*43*–*45*), and chimeric HAs containing exotic head domains from avian influenza virus subtypes with group 1 or 2 stem domains (*46*–*48*). We developed a headless HA immunogen with stabilized stem proteins multimerized on ferritin nanoparticles (*21*). After two doses of the H1ssF immunogen given without adjuvant 16 weeks apart, we observed a strong HA stem–specific plasmablast and memory B cell response after the first dose and a reduced but detectable memory B cell boost after the second dose. HA stem–specific memory B cells remained twofold higher than baseline at 7 months after the first immunization. The response to the vaccine appeared to be primarily an expansion of preexisting memory B cells, because Igs expressed by the early plasmablast and memory B cell response were isotype-switched and somatically mutated. Reduced responses to a second vaccine dose have been observed in other vaccine studies when there is preexisting immunity (*49*, *50*). These include a phase 1 trial with group 1 chimeric H8/1N1 and H5/1N1 split virion inactivated vaccines recently reported that also boosted H1 stem–specific responses, especially after addition of an AS03 adjuvant (*29*, *49*, *51*).

One of the most notable findings when H1 stem–specific mAbs were first widely characterized was the identification of a broadly neutralizing convergent class of Igs encoded by VH1-69 that dominated the H1 stem response and bound to a central epitope on the

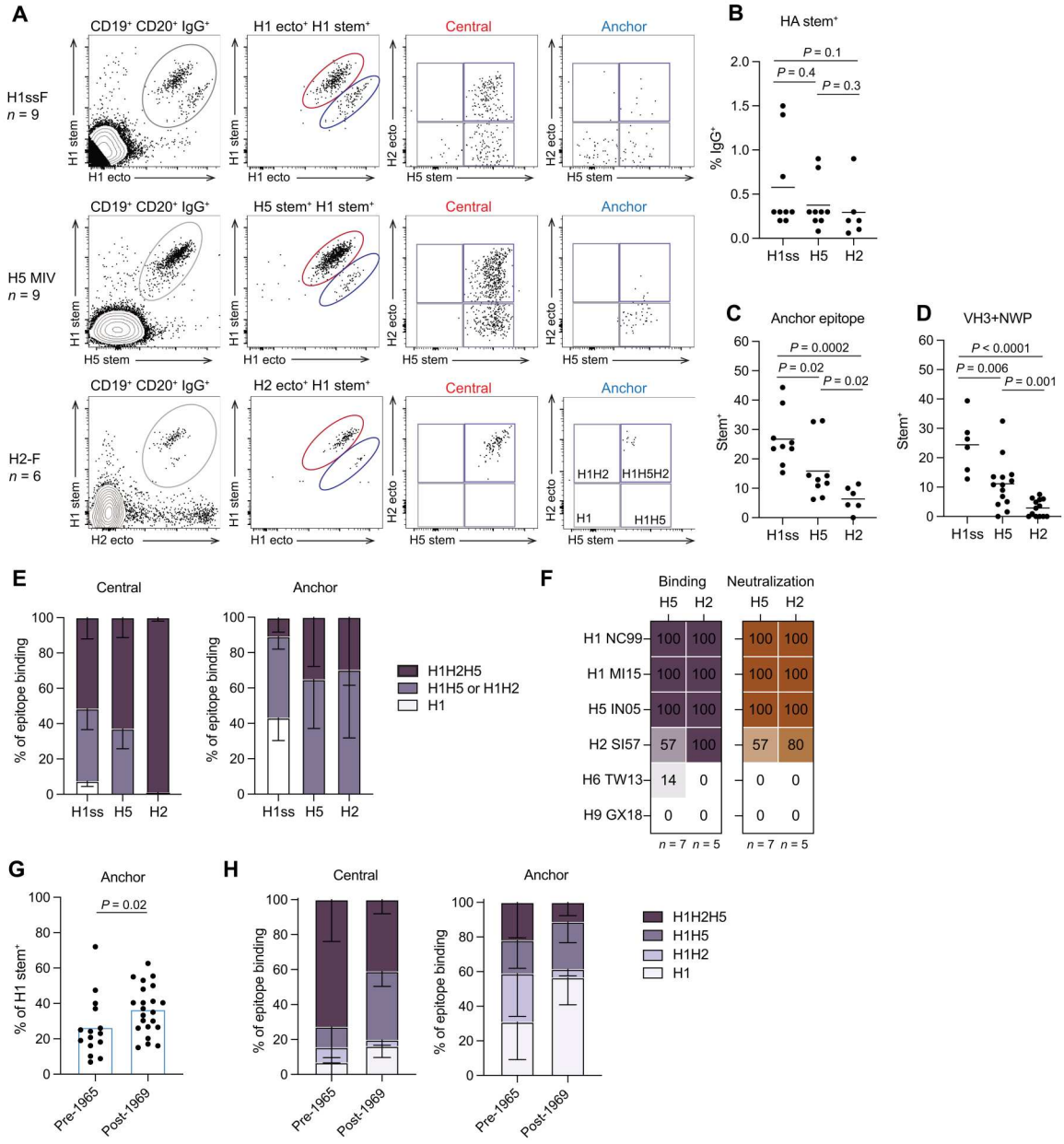

Fig. 6. Vaccination with H5 or H2 elicits fewer anchor epitope–binding B cells. (**A**) Representative flow cytometry plots used to detect and characterize HA stem–specific memory B cells in PBMCs after H1ssF, H5 MIV, or H2-np vaccination. $CD19^+$ $CD20^+$ IgG^+ memory B cells were first gated as in fig. S6A. H1 stem, H1H5 stem, or H1H2 $stem^+$ B cells were gated, and cells binding to the central epitope (upper H1 $ectodomain^+$ H1 $stem^+$ population) or anchor epitope (lower H1 $ectodomain^+$ H1 $stem^+$ population) were further analyzed for the capacity to cross-react with an H2 HA ectodomain or H5 stem as in fig. S6B. The number of participants analyzed for each vaccine group is indicated below the vaccine name. (**B** and **C**) Proportions of IgG^+ memory B cells double-positive for both the vaccinating strain and H1 stem (B) and proportions of HA stem–specific IgG^+ memory B cells in the lower population binding the anchor epitope (C). (**D**) HA stem–specific IgG^+ memory B cells were single cell–sorted, and Ig sequences were amplified and sequenced. The proportion of all HA stem–specific cells that belong to the VH3+NWP class is shown. In (B) to (D), each dot represents the proportion in each individual, with the line indicating the mean. (**E**) Proportion of IgG^+ memory B cells binding the central epitope (left) or anchor epitope (right) that cross-react with H5, H2 HA, or both as indicated. The mean and SD of the proportion of memory B cells with the indicated cross-reactivity for each vaccine group are shown. (**F**) Proportion of mAbs from VH3+NWP class Ig sequences isolated from IgG memory B cells after H5 or H2 vaccination that could bind or neutralize the indicated influenza strains. Binding and neutralization for each mAb is shown in fig. S9B. (**G**) Proportion of H1 stem–specific IgG^+ memory B cells that recognized the anchor epitope 2 weeks after the first H1ssF dose in participants who were born before 1965 ($n = 15$) or after 1969 ($n = 22$) as indicated. The bars indicate the mean. (**H**) Cross-reactivity of anchor and central epitope H1 stem–binding IgG memory B cells was tested by flow cytometry for a subset of individuals in (G). The mean and SD of the proportion of memory B cells with the indicated cross-reactivity for each age group are shown. $n = 8$ for the pre-1965 group; $n = 13$ for the post-1969 group. Statistical significance in (B) to (D) and (G) was determined by unpaired Mann-Whitney *t* test.

stem (*3*, *4*, *9*, *13*–*15*, *52*–*54*). In response to the H1ssF immunogen, more than 50% of the expanded plasmablasts and memory B cells expressed VH1-69 class Igs, equivalent to the response to group 1 immunogens with naturally encoded HAs containing both head and stem domains (*3*, *15*, *16*). Previously described multidonor Ig classes encoded by VH1-18 and VH6-1 were also identified in a subset of individuals after H1ssF vaccination (*33*, *34*).

Although the majority of the H1 stem–specific response to H1ssF recognized the central stem epitope, a third of serum Abs and B cells bound a second epitope proximal to the viral membrane. This region of the ectodomain just above the anchor domain was recently recognized as a common target of H1 stem–specific B cells after vaccination with both seasonal QIV and AS03 adjuvanted chimeric H5/1-inactivated vaccines (*29*). Similar to Guthmiller *et al.* (*29*), we found that H1 stem–specific B cells binding this epitope expressed Igs with a highly restricted VH/VL signature that was pervasive throughout the 20 H1ssF- and 6 QIV-vaccinated individuals whose Ig repertoire was analyzed. B cells binding the anchor epitope were most commonly limited to H1 reactivity, with few able to neutralize other group 1 influenza subtypes. In addition, although anchor Abs showed remarkable breadth of binding and neutralization across H1 influenza strains, their neutralization potency was reduced to more distant H1 strains, whereas central binding B cells showed equivalent potency across H1 strains. This suggests that anchor binding Abs may have more limited efficacy in the context of a pandemic with different subtypes or antigenically shifted H1 strains. Structurally, it is unclear why Abs binding this region would have more limited breadth, because this epitope is highly conserved across group 1 subtypes (*29*). Vaccination with H2 or H5 immunogens did elicit B cells binding the anchor epitope capable of neutralizing these subtypes, but their frequency was substantially reduced, indicating that it may be more difficult to form Igs with greater breadth of binding to this epitope. Overall, H2 and H5 immunogens elicited stem-reactive memory B cells with greater breadth. For this reason, we may be able to achieve even broader neutralizing Ab responses using an H5 or H2 stabilized stem immunogen instead of H1. However, because B cells almost exclusively targeted the central epitope with H5 or H2 immunogens, the response would be more vulnerable to potential escape mutations in this region.

Although roughly a third of the B cell response to H1ssF targeted the anchor epitope on average, the proportion varied considerably from participant to participant. Although all the factors that contribute to this variation are unclear, differences in previous influenza exposure history most likely play a role. Abs targeting the anchor epitope showed very reduced capacity to neutralize H2 and pre-1957 H1 strains and were poorly elicited by H2 vaccination. In individuals born between 1951 and 1964 whose first exposure to group 1 influenza virus would have been H2 or pre-1957 H1 strains, proportionally fewer anchor-targeted B cells expanded after H1ssF vaccination. This suggests that their memory B cell repertoire, shaped by these early influenza strain exposures, includes fewer B cells recognizing this lower epitope. Encouragingly, however, the total magnitude of the H1 stem–specific B cell response was not lower in older individuals, and their overall H1 stem–specific response to H1ssF was more cross-reactive than in younger individuals both because it focused more on the central epitope and because central epitope–binding B cells in older individuals were more cross-reactive.

One concern with this stabilized stem immunogen was whether it would be antigenically intact and elicit similar stem-directed responses as naturally formed HAs. It was shown previously, for example, that headless mini-HAs could not bind anchor binding Abs in soluble form, although they could when membrane-bound (*29*). Abs recognizing the anchor region could bind both the H1 stabilized stem soluble trimers and ferritin nanoparticles, indicating that both forms were antigenically intact in this region. In addition, vaccination with H1ssF elicited an H1 stem–specific B cell response that was higher than QIV vaccination but qualitatively very similar, providing further evidence of this stem immunogen being antigenically similar to the stem domain on naturally formed HA.

Our evaluation of the B cell response to H1ssF in this phase 1 first-in-human study has limitations, including the relatively low number of participants enrolled from one geographical area. Future studies with a larger and more genetically diverse cohort will be needed to fully understand the response in the human population worldwide. Large-scale studies will also be needed to assess the protective effect of HA stem–directed Abs elicited by this immunogen upon infection. Furthermore, our assessment of the B cell response was limited to memory B cell responses in peripheral blood and did not address whether affinity maturation occurred to the H1 NC99 viral strain. To understand the potential for long-term Ab responses, we would need to evaluate the expansion of long-lived H1 stem–specific plasma cells in the bone marrow. In conclusion, we found that the H1ssF immunogen boosts broadly neutralizing stem-directed serological Abs and memory B cells targeting conserved regions on the HA stem. Addition of adjuvants will likely boost these responses even further and has the potential to provide much needed protection against severe disease in the context of high-risk populations during yearly influenza epidemics or pandemics.

MATERIALS AND METHODS

Study design

The H1ssF vaccine study (ClinicalTrials.gov identifier NCT03814720), H5 vaccine study (*35*, *55*) (ClinicalTrials.gov identifier NCT01086657), H2 vaccine study (*19*) (ClinicalTrials.gov identifier NCT03186781), and 2020–2021 QIV vaccine study (ClinicalTrials.gov identifier NCT01132859) were conducted at the National Institutes of Health (NIH) Clinical Center by the Vaccine Research Center (VRC) Clinical Trials Program, National Institute of Allergy and Infectious Disease (NIAID), NIH in Bethesda, MD. The trial protocols were reviewed and approved by the NIAID Institutional Review Board. Informed consent was obtained from every enrolled participant and complied with all relevant ethical regulations. Compensation was given for time and effort related to participation in the clinical trial. The H1ssF, H5, and H2 vaccine studies were phase 1 open-label clinical trials in healthy adults designed to study the safety, tolerability, and immunogenicity of prime-boost vaccination regimens. Primary study end points for the H1ssF, H5, and H2 studies are reported elsewhere (*19*, *35*, *56*). Sample size, randomization, and inclusion/exclusion criteria were determined on the basis of the primary trial end points and not the exploratory analysis reported here. The studies were not blinded.

In the H1ssF study, participants were vaccinated with either one 20-μg dose or two 60-μg doses of an H1 stabilized stem ferritin

nanoparticle administered 16 weeks apart. Participants who received the 60-μg doses were further stratified into different age groups between 18 and 70 years old. For the H5N1 vaccine study samples, only participants vaccinated with two doses given 24 weeks apart of monovalent influenza subunit virion (A/Indonesia/05/2005) vaccine (MIV) manufactured by Sanofi Pasteur Inc. were included in this study. For the H2 vaccine study samples, only participants vaccinated with two doses of H2 HA ferritin nanoparticle 16 weeks apart were included. In the 2020–2021 QIV vaccine study, healthy adults aged 18 to 50 who had not yet received the 2020–2021 seasonal influenza vaccine received the 2020–2021 Flucelvax in fall of 2020. Study participant demographics are provided in table S1.

Statistical analysis

All raw, individual-level data for experiments where $n < 20$ are presented in data file S1. Statistical analysis was performed with GraphPad Prism 8.0. Specific details of statistical analysis are indicated in the figure legends and Results. *P* values equal to or below 0.05 were considered significant. Normality tests were conducted on all data to determine the appropriate statistical test. All statistical tests used are two-tailed.

Supplementary Materials

This PDF file includes:
Materials and Methods
Figs. S1 to S9
Tables S1 and S2
References (*57*–*77*)

Other Supplementary Material for this manuscript includes the following:
Data file S1
MDAR Reproducibility Checklist

View/request a protocol for this paper from *Bio-protocol*.

REFERENCES AND NOTES

1. A. D. Iuliano, K. M. Roguski, H. H. Chang, D. J. Muscatello, R. Palekar, S. Tempia, C. Cohen, J. M. Gran, D. Schanzer, B. J. Cowling, P. Wu, J. Kyncl, L. W. Ang, M. Park, M. Redlberger-Fritz, H. Yu, L. Espenhain, A. Krishnan, G. Emukule, L. van Asten, S. P. da Silva, S. Aungkulanon, U. Buchholz, M. A. Widdowson, J. S. Bresee; Global Seasonal Influenza-associated Mortality Collaborator Network, Estimates of global seasonal influenza-associated respiratory mortality: A modelling study. *Lancet* **391**, 1285–1300 (2018).
2. M. Kanekiyo, B. S. Graham, Next-generation influenza vaccines. *Cold Spring Harb. Perspect. Med.* **11**, a038448 (2021).
3. S. F. Andrews, Y. Huang, K. Kaur, L. I. Popova, I. Y. Ho, N. T. Pauli, C. J. Henry Dunand, W. M. Taylor, S. Lim, M. Huang, X. Qu, J. H. Lee, M. Salgado-Ferrer, F. Krammer, P. Palese, J. Wrammert, R. Ahmed, P. C. Wilson, Immune history profoundly affects broadly protective B cell responses to influenza. *Sci. Transl. Med.* **7**, 316ra192 (2015).
4. G. M. Li, C. Chiu, J. Wrammert, M. McCausland, S. F. Andrews, N. Y. Zheng, J. H. Lee, M. Huang, X. Qu, S. Edupuganti, M. Mulligan, S. R. Das, J. W. Yewdell, A. K. Mehta, P. C. Wilson, R. Ahmed, Pandemic H1N1 influenza vaccine induces a recall response in humans that favors broadly cross-reactive memory B cells. *Proc. Natl. Acad. Sci. U.S.A.* **109**, 9047–9052 (2012).
5. Y. Okuno, Y. Isegawa, F. Sasao, S. Ueda, A common neutralizing epitope conserved between the hemagglutinins of influenza A virus H1 and H2 strains. *J. Virol.* **67**, 2552–2558 (1993).
6. H. Sagawa, A. Ohshima, I. Kato, Y. Okuno, Y. Isegawa, The immunological activity of a deletion mutant of influenza virus haemagglutinin lacking the globular region. *J. Gen. Virol.* **77**, 1483–1487 (1996).
7. D. C. Ekiert, G. Bhabha, M. A. Elsliger, R. H. Friesen, M. Jongeneelen, M. Throsby, J. Goudsmit, I. A. Wilson, Antibody recognition of a highly conserved influenza virus epitope. *Science* **324**, 246–251 (2009).
8. J. Sui, W. C. Hwang, S. Perez, G. Wei, D. Aird, L. M. Chen, E. Santelli, B. Stec, G. Cadwell, M. Ali, H. Wan, A. Murakami, A. Yammanuru, T. Han, N. J. Cox, L. A. Bankston, R. O. Donis, R. C. Liddington, W. A. Marasco, Structural and functional bases for broad-spectrum neutralization of avian and human influenza A viruses. *Nat. Struct. Mol. Biol.* **16**, 265–273 (2009).
9. J. Wrammert, D. Koutsonanos, G. M. Li, S. Edupuganti, J. Sui, M. Morrissey, M. McCausland, I. Skountzou, M. Hornig, W. I. Lipkin, A. Mehta, B. Razavi, C. Del Rio, N. Y. Zheng, J. H. Lee, M. Huang, Z. Ali, K. Kaur, S. Andrews, R. R. Amara, Y. Wang, S. R. Das, C. D. O'Donnell, J. W. Yewdell, K. Subbarao, W. A. Marasco, M. J. Mulligan, R. Compans, R. Ahmed, P. C. Wilson, Broadly cross-reactive antibodies dominate the human B cell response against 2009 pandemic H1N1 influenza virus infection. *J. Exp. Med.* **208**, 181–193 (2011).
10. C. A. Thomson, Y. Wang, L. M. Jackson, M. Olson, W. Wang, A. Liavonchanka, L. Keleta, V. Silva, S. Diederich, R. B. Jones, J. Gubbay, J. Pasick, M. Petric, F. Jean, V. G. Allen, E. G. Brown, J. M. Rini, J. W. Schrader, Pandemic H1N1 influenza infection and vaccination in humans induces cross-protective antibodies that target the hemagglutinin stem. *Front. Immunol.* **3**, 87 (2012).
11. M. S. Miller, T. Tsibane, F. Krammer, R. Hai, S. Rahmat, C. F. Basler, P. Palese, 1976 and 2009 H1N1 influenza virus vaccines boost anti-hemagglutinin stalk antibodies in humans. *J. Infect. Dis.* **207**, 98–105 (2013).
12. L. Liu, R. Nachbagauer, L. Zhu, Y. Huang, X. Xie, S. Jin, A. Zhang, Y. Wan, A. Hirsh, D. Tian, X. Shi, Z. Dong, S. Yuan, Y. Hu, F. Krammer, X. Zhang, J. Xu, Induction of broadly cross-reactive stalk-specific antibody responses to influenza group 1 and group 2 hemagglutinins by natural H7N9 virus infection in humans. *J. Infect. Dis.* **215**, 518–528 (2017).
13. A. H. Ellebedy, F. Krammer, G. M. Li, M. S. Miller, C. Chiu, J. Wrammert, C. Y. Chang, C. W. Davis, M. McCausland, R. Elbein, S. Edupuganti, P. Spearman, S. F. Andrews, P. C. Wilson, A. Garcia-Sastre, M. J. Mulligan, A. K. Mehta, P. Palese, R. Ahmed, Induction of broadly cross-reactive antibody responses to the influenza HA stem region following H5N1 vaccination in humans. *Proc. Natl. Acad. Sci. U.S.A.* **111**, 13133–13138 (2014).
14. A. K. Wheatley, J. R. Whittle, D. Lingwood, M. Kanekiyo, H. M. Yassine, S. S. Ma, S. R. Narpala, M. S. Prabhakaran, R. A. Matus-Nicodemos, R. T. Bailer, G. J. Nabel, B. S. Graham, J. E. Ledgerwood, R. A. Koup, A. B. McDermott, H5N1 vaccine-elicited memory B cells are genetically constrained by the IGHV locus in the recognition of a neutralizing epitope in the hemagglutinin stem. *J. Immunol.* **195**, 602–610 (2015).
15. S. F. Andrews, M. G. Joyce, M. J. Chambers, R. A. Gillespie, M. Kanekiyo, K. Leung, E. S. Yang, Y. Tsybovsky, A. K. Wheatley, M. C. Crank, J. C. Boyington, M. S. Prabhakaran, S. R. Narpala, X. Chen, R. T. Bailer, G. Chen, E. Coates, P. D. Kwong, R. A. Koup, J. R. Mascola, B. S. Graham, J. E. Ledgerwood, A. B. McDermott, Preferential induction of cross-group influenza A hemagglutinin stem-specific memory B cells after H7N9 immunization in humans. *Sci. Immunol.* **2**, eaan2676 (2017).
16. S. F. Andrews, J. E. Raab, J. Gorman, R. A. Gillespie, C. S. F. Cheung, R. Rawi, L. Y. Cominsky, J. C. Boyington, A. Creanga, C. H. Shen, D. R. Harris, A. S. Olia, A. F. Nazzari, T. Zhou, K. V. Houser, G. L. Chen, J. R. Mascola, B. S. Graham, M. Kanekiyo, J. E. Ledgerwood, P. D. Kwong, A. B. McDermott, A single residue in influenza virus H2 hemagglutinin enhances the breadth of the B cell response elicited by H2 vaccination. *Nat. Med.* **28**, 373–382 (2022).
17. R. Nachbagauer, B. Salaun, D. Stadlbauer, M. A. Behzadi, D. Friel, A. Rajabhathor, A. Choi, R. A. Albrecht, M. Debois, A. Garcia-Sastre, R. N. Rouxel, W. Sun, P. Palese, C. P. Mallett, B. L. Innis, F. Krammer, C. Claeys, Pandemic influenza virus vaccines boost hemagglutinin stalk-specific antibody responses in primed adult and pediatric cohorts. *NPJ Vaccines* **4**, 51 (2019).
18. J. Han, A. J. Schmitz, S. T. Richey, Y. N. Dai, H. L. Turner, B. M. Mohammed, D. H. Fremont, A. H. Ellebedy, A. B. Ward, Polyclonal epitope mapping reveals temporal dynamics and diversity of human antibody responses to H5N1 vaccination. *Cell Rep.* **34**, 108682 (2021).
19. K. V. Houser, G. L. Chen, C. Carter, M. C. Crank, T. A. Nguyen, M. C. B. Florez, N. M. Berkowitz, F. Mendoza, C. S. Hendel, I. J. Gordon, E. E. Coates, S. Vazquez, J. Stein, C. L. Case, H. Lawlor, K. Carlton, M. R. Gaudinski, L. Strom, A. R. Hofstetter, C. J. Liang, S. Narpala, C. Hatcher, R. A. Gillespie, A. Creanga, M. Kanekiyo, J. E. Raab, S. F. Andrews, Y. Zhang, E. S. Yang, L. Wang, K. Leung, W. P. Kong, A. W. Freyn, R. Nachbagauer, P. Palese, R. T. Bailer, A. B. McDermott, R. A. Koup, J. G. Gall, F. Arnold, J. R. Mascola, B. S. Graham, J. E. Ledgerwood; VRC 316 Study Team, Safety and immunogenicity of a ferritin nanoparticle H2 influenza vaccine in healthy adults: A phase 1 trial. *Nat. Med.* **28**, 383–391 (2022).
20. S. F. Andrews, M. J. Chambers, C. A. Schramm, J. Plyler, J. E. Raab, M. Kanekiyo, R. A. Gillespie, A. Ransier, S. Darko, J. Hu, X. Chen, H. M. Yassine, J. C. Boyington, M. C. Crank, G. L. Chen, E. Coates, J. R. Mascola, D. C. Douek, B. S. Graham, J. E. Ledgerwood, A. B. McDermott, Activation dynamics and immunoglobulin evolution of pre-existing and newly generated

human memory B cell responses to influenza hemagglutinin. *Immunity* **51**, 398–410.e5 (2019).
21. H. M. Yassine, J. C. Boyington, P. M. McTamney, C. J. Wei, M. Kanekiyo, W. P. Kong, J. R. Gallagher, L. Wang, Y. Zhang, M. G. Joyce, D. Lingwood, S. M. Moin, H. Andersen, Y. Okuno, S. S. Rao, A. K. Harris, P. D. Kwong, J. R. Mascola, G. J. Nabel, B. S. Graham, Hemagglutinin-stem nanoparticles generate heterosubtypic influenza protection. *Nat. Med.* **21**, 1065–1070 (2015).
22. M. Kanekiyo, C. J. Wei, H. M. Yassine, P. M. McTamney, J. C. Boyington, J. R. Whittle, S. S. Rao, W. P. Kong, L. Wang, G. J. Nabel, Self-assembling influenza nanoparticle vaccines elicit broadly neutralizing H1N1 antibodies. *Nature* **499**, 102–106 (2013).
23. H. E. Mei, T. Yoshida, W. Sime, F. Hiepe, K. Thiele, R. A. Manz, A. Radbruch, T. Dorner, Blood-borne human plasma cells in steady state are derived from mucosal immune responses. *Blood* **113**, 2461–2469 (2009).
24. K. E. Neu, J. J. Guthmiller, M. Huang, J. La, M. C. Vieira, K. Kim, N. Y. Zheng, M. Cortese, M. E. Tepora, N. J. Hamel, K. T. Rojas, C. Henry, D. Shaw, C. L. Dulberger, B. Pulendran, S. Cobey, A. A. Khan, P. C. Wilson, Spec-seq unveils transcriptional subpopulations of antibody-secreting cells following influenza vaccination. *J. Clin. Invest.* **129**, 93–105 (2019).
25. C. J. Henry Dunand, P. C. Wilson, Restricted, canonical, stereotyped and convergent immunoglobulin responses. *Philos. Trans. R Soc. Lond. B Biol. Sci.* **370**, 20140238 (2015).
26. S. F. Andrews, B. S. Graham, J. R. Mascola, A. B. McDermott, Is it possible to develop a "Universal" influenza virus vaccine? immunogenetic considerations underlying B-cell biology in the development of a pan-subtype influenza a vaccine targeting the hemagglutinin stem. *Cold Spring Harb. Perspect. Biol.* **10**, a029413 (2017).
27. D. Lingwood, P. M. McTamney, H. M. Yassine, J. R. Whittle, X. Guo, J. C. Boyington, C. J. Wei, G. J. Nabel, Structural and genetic basis for development of broadly neutralizing influenza antibodies. *Nature* **489**, 566–570 (2012).
28. L. Pappas, M. Foglierini, L. Piccoli, N. L. Kallewaard, F. Turrini, C. Silacci, B. Fernandez-Rodriguez, G. Agatic, I. Giacchetto-Sasselli, G. Pellicciotta, F. Sallusto, Q. Zhu, E. Vicenzi, D. Corti, A. Lanzavecchia, Rapid development of broadly influenza neutralizing antibodies through redundant mutations. *Nature* **516**, 418–422 (2014).
29. J. J. Guthmiller, J. Han, H. A. Utset, L. Li, L. Y. Lan, C. Henry, C. T. Stamper, M. McMahon, G. O'Dell, M. L. Fernandez-Quintero, A. W. Freyn, F. Amanat, O. Stovicek, L. Gentles, S. T. Richey, A. T. de la Pena, V. Rosado, H. L. Dugan, N. Y. Zheng, M. E. Tepora, D. J. Bitar, S. Changrob, S. Strohmeier, M. Huang, A. Garcia-Sastre, K. R. Liedl, J. D. Bloom, R. Nachbagauer, P. Palese, F. Krammer, L. Coughlan, A. B. Ward, P. C. Wilson, Broadly neutralizing antibodies target a haemagglutinin anchor epitope. *Nature* **602**, 314–320 (2022).
30. D. J. Benton, A. Nans, L. J. Calder, J. Turner, U. Neu, Y. P. Lin, E. Ketelaars, N. L. Kallewaard, D. Corti, A. Lanzavecchia, S. J. Gamblin, P. B. Rosenthal, J. J. Skehel, Influenza hemagglutinin membrane anchor. *Proc. Natl. Acad. Sci. U.S.A.* **115**, 10112–10117 (2018).
31. C. J. Wei, J. C. Boyington, P. M. McTamney, W. P. Kong, M. B. Pearce, L. Xu, H. Andersen, S. Rao, T. M. Tumpey, Z. Y. Yang, G. J. Nabel, Induction of broadly neutralizing H1N1 influenza antibodies by vaccination. *Science* **329**, 1060–1064 (2010).
32. C. Dreyfus, N. S. Laursen, T. Kwaks, D. Zuijdgeest, R. Khayat, D. C. Ekiert, J. H. Lee, Z. Metlagel, M. V. Bujny, M. Jongeneelen, R. van der Vlugt, M. Lamrani, H. J. Korse, E. Geelen, O. Sahin, M. Sieuwerts, J. P. Brakenhoff, R. Vogels, O. T. Li, L. L. Poon, M. Peiris, W. Koudstaal, A. B. Ward, I. A. Wilson, J. Goudsmit, R. H. Friesen, Highly conserved protective epitopes on influenza B viruses. *Science* **337**, 1343–1348 (2012).
33. M. G. Joyce, A. K. Wheatley, P. V. Thomas, G. Y. Chuang, C. Soto, R. T. Bailer, A. Druz, I. S. Georgiev, R. A. Gillespie, M. Kanekiyo, W. P. Kong, K. Leung, S. N. Narpala, M. S. Prabhakaran, E. S. Yang, B. Zhang, Y. Zhang, M. Asokan, J. C. Boyington, T. Bylund, S. Darko, C. R. Lees, A. Ransier, C. H. Shen, L. Wang, J. R. Whittle, X. Wu, H. M. Yassine, C. Santos, Y. Matsuoka, Y. Tsybovsky, U. Baxa, N. C. S. Program, J. C. Mullikin, K. Subbarao, D. C. Douek, B. S. Graham, R. A. Koup, J. E. Ledgerwood, M. Roederer, L. Shapiro, P. D. Kwong, J. R. Mascola, A. B. McDermott, Vaccine-induced antibodies that neutralize group 1 and group 2 influenza a viruses. *Cell* **166**, 609–623 (2016).
34. N. L. Kallewaard, D. Corti, P. J. Collins, U. Neu, J. M. McAuliffe, E. Benjamin, L. Wachter-Rosati, F. J. Palmer-Hill, A. Q. Yuan, P. A. Walker, M. K. Vorlaender, S. Bianchi, B. Guarino, A. De Marco, F. Vanzetta, G. Agatic, M. Foglierini, D. Pinna, B. Fernandez-Rodriguez, A. Fruehwirth, C. Silacci, R. W. Ogrodowicz, S. R. Martin, F. Sallusto, J. A. Suzich, A. Lanzavecchia, Q. Zhu, S. J. Gamblin, J. J. Skehel, Structure and function analysis of an antibody recognizing all influenza a subtypes. *Cell* **166**, 596–608 (2016).
35. J. E. Ledgerwood, K. Zephir, Z. Hu, C. J. Wei, L. Chang, M. E. Enama, C. S. Hendel, S. Sitar, R. T. Bailer, R. A. Koup, J. R. Mascola, G. J. Nabel, B. S. Graham; VRC 310 Study Team, Prime-boost interval matters: A randomized phase 1 study to identify the minimum interval necessary to observe the H5 DNA influenza vaccine priming effect. *J. Infect. Dis.* **208**, 418–422 (2013).
36. M. Throsby, E. van den Brink, M. Jongeneelen, L. L. Poon, P. Alard, L. Cornelissen, A. Bakker, F. Cox, E. van Deventer, Y. Guan, J. Cinatl, J. ter Meulen, I. Lasters, R. Carsetti, M. Peiris, J. de Kruif, J. Goudsmit, Heterosubtypic neutralizing monoclonal antibodies cross-protective against H5N1 and H1N1 recovered from human IgM$^+$ memory B cells. *PLOS ONE* **3**, e3942 (2008).
37. S. Ng, R. Nachbagauer, A. Balmaseda, D. Stadlbauer, S. Ojeda, M. Patel, A. Rajabhathor, R. Lopez, A. F. Guglia, N. Sanchez, F. Amanat, L. Gresh, G. Kuan, F. Krammer, A. Gordon, Novel correlates of protection against pandemic H1N1 influenza A virus infection. *Nat. Med.* **25**, 962–967 (2019).
38. S. R. Christensen, S. A. Toulmin, T. Griesman, L. E. Lamerato, J. G. Petrie, E. T. Martin, A. S. Monto, S. E. Hensley, Assessing the protective potential of H1N1 influenza virus hemagglutinin head and stalk antibodies in humans. *J. Virol.* **93**, e02134-18 (2019).
39. T. Aydillo, A. Escalera, S. Strohmeier, S. Aslam, J. Sanchez-Cespedes, J. Ayllon, C. Roca-Oporto, P. Perez-Romero, M. Montejo, J. Gavalda, P. Munoz, F. Lopez-Medrano, J. Carratala, F. Krammer, A. Garcia-Sastre, E. Cordero, Pre-existing hemagglutinin stalk antibodies correlate with protection of lower respiratory symptoms in flu-infected transplant patients. *Cell Rep. Med.* **1**, 100130 (2020).
40. J. K. Park, A. Han, L. Czajkowski, S. Reed, R. Athota, T. Bristol, L. A. Rosas, A. Cervantes-Medina, J. K. Taubenberger, M. J. Memoli, Evaluation of preexisting anti-hemagglutinin stalk antibody as a correlate of protection in a healthy volunteer challenge with influenza A/H1N1pdm virus. *MBio* **9**, e02284-17 (2018).
41. S. A. Valkenburg, V. V. Mallajosyula, O. T. Li, A. W. Chin, G. Carnell, N. Temperton, R. Varadarajan, L. L. Poon, Stalking influenza by vaccination with pre-fusion headless HA mini-stem. *Sci. Rep.* **6**, 22666 (2016).
42. V. V. Mallajosyula, M. Citron, F. Ferrara, N. J. Temperton, X. Liang, J. A. Flynn, R. Varadarajan, Hemagglutinin sequence conservation guided stem immunogen design from influenza A H3 subtype. *Front. Immunol.* **6**, 329 (2015).
43. K. S. Corbett, S. M. Moin, H. M. Yassine, A. Cagigi, M. Kanekiyo, S. Boyoglu-Barnum, S. I. Myers, Y. Tsybovsky, A. K. Wheatley, C. A. Schramm, R. A. Gillespie, W. Shi, L. Wang, Y. Zhang, S. F. Andrews, M. G. Joyce, M. C. Crank, D. C. Douek, A. B. McDermott, J. R. Mascola, B. S. Graham, J. C. Boyington, Design of nanoparticulate group 2 influenza virus hemagglutinin stem antigens that activate unmutated ancestor B cell receptors of broadly neutralizing antibody lineages. *MBio* **10**, e02810-18 (2019).
44. A. Impagliazzo, F. Milder, H. Kuipers, M. V. Wagner, X. Zhu, R. M. Hoffman, R. van Meersbergen, J. Huizingh, P. Wanningen, J. Verspuij, M. de Man, Z. Ding, A. Apetri, B. Kükrer, E. Sneekes-Vriese, D. Tomkiewicz, N. S. Laursen, P. S. Lee, A. Zakrzewska, L. Dekking, J. Tolboom, L. Tettero, S. van Meerten, W. Yu, W. Koudstaal, J. Goudsmit, A. B. Ward, W. Meijberg, I. A. Wilson, K. Radošević, A stable trimeric influenza hemagglutinin stem as a broadly protective immunogen. *Science* **349**, 1301–1306 (2015).
45. J. Steel, A. C. Lowen, T. T. Wang, M. Yondola, Q. Gao, K. Haye, A. Garcia-Sastre, P. Palese, Influenza virus vaccine based on the conserved hemagglutinin stalk domain. *MBio* **1**, e00018-10 (2010).
46. F. Krammer, I. Margine, R. Hai, A. Flood, A. Hirsh, V. Tsvetnitsky, D. Chen, P. Palese, H3 stalk-based chimeric hemagglutinin influenza virus constructs protect mice from H7N9 challenge. *J. Virol.* **88**, 2340–2343 (2014).
47. F. Krammer, N. Pica, R. Hai, I. Margine, P. Palese, Chimeric hemagglutinin influenza virus vaccine constructs elicit broadly protective stalk-specific antibodies. *J. Virol.* **87**, 6542–6550 (2013).
48. R. Nachbagauer, W. C. Liu, A. Choi, T. J. Wohlbold, T. Atlas, M. Rajendran, A. Solórzano, F. Berlanda-Scorza, A. Garcia-Sastre, P. Palese, R. A. Albrecht, F. Krammer, A universal influenza virus vaccine candidate confers protection against pandemic H1N1 infection in preclinical ferret studies. *NPJ Vaccines* **2**, 26 (2017).
49. R. Nachbagauer, J. Feser, A. Naficy, D. I. Bernstein, J. Guptill, E. B. Walter, F. Berlanda-Scorza, D. Stadlbauer, P. C. Wilson, T. Aydillo, M. A. Behzadi, D. Bhavsar, C. Bliss, C. Capuano, J. M. Carreno, V. Chromikova, C. Claeys, L. Coughlan, A. W. Freyn, C. Gast, A. Javier, K. Jiang, C. Mariottini, M. McMahon, M. McNeal, A. Solorzano, S. Strohmeier, W. Sun, M. Van der Wielen, B. L. Innis, A. Garcia-Sastre, P. Palese, F. Krammer, A chimeric hemagglutinin-based universal influenza virus vaccine approach induces broad and long-lasting immunity in a randomized, placebo-controlled phase I trial. *Nat. Med.* **27**, 106–114 (2021).
50. E. Phung, L. A. Chang, M. Mukhamedova, L. Yang, D. Nair, S. A. Rush, K. M. Morabito, J. S. McLellan, U. J. Buchholz, J. R. Mascola, M. C. Crank, G. Chen, B. S. Graham, T. J. Ruckwardt, Elicitation of pneumovirus-specific B cell responses by a prefusion-stabilized respiratory syncytial virus F subunit vaccine. *Sci. Transl. Med.* **14**, eabo5032 (2022).
51. D. I. Bernstein, J. Guptill, A. Naficy, R. Nachbagauer, F. Berlanda-Scorza, J. Feser, P. C. Wilson, A. Solorzano, M. Van der Wielen, E. B. Walter, R. A. Albrecht, K. N. Buschle, Y. Q. Chen, C. Claeys, M. Dickey, H. L. Dugan, M. E. Ermler, D. Freeman, M. Gao, C. Gast, J. J. Guthmiller, R. Hai, C. Henry, L. Y. Lan, M. McNeal, A. E. Palm, D. G. Shaw, C. T. Stamper, W. Sun, V. Sutton, M. E. Tepora, R. Wahid, H. Wenzel, T. J. Wohlbold, B. L. Innis, A. Garcia-Sastre, P. Palese, F. Krammer, Immunogenicity of chimeric haemagglutinin-based, universal influenza virus vaccine candidates: Interim results of a randomised, placebo-controlled, phase 1 clinical trial. *Lancet Infect. Dis.* **20**, 80–91 (2020).
52. Y. Avnir, C. T. Watson, J. Glanville, E. C. Peterson, A. S. Tallarico, A. S. Bennett, K. Qin, Y. Fu, C. Y. Huang, J. H. Beigel, F. Breden, Q. Zhu, W. A. Marasco, *IGHV1-69* polymorphism

modulates anti-influenza antibody repertoires, correlates with IGHV utilization shifts and varies by ethnicity. *Sci. Rep.* **6**, 20842 (2016).
53. B. Cortina-Ceballos, E. E. Godoy-Lozano, J. Tellez-Sosa, M. Ovilla-Munoz, H. Samano-Sanchez, A. Aguilar-Salgado, R. E. Gomez-Barreto, H. Valdovinos-Torres, I. Lopez-Martinez, R. Aparicio-Antonio, M. H. Rodriguez, J. Martinez-Barnetche, Longitudinal analysis of the peripheral B cell repertoire reveals unique effects of immunization with a new influenza virus strain. *Genome Med.* **7**, 124 (2015).
54. J. R. Whittle, A. K. Wheatley, L. Wu, D. Lingwood, M. Kanekiyo, S. S. Ma, S. R. Narpala, H. M. Yassine, G. M. Frank, J. W. Yewdell, J. E. Ledgerwood, C. J. Wei, A. B. McDermott, B. S. Graham, R. A. Koup, G. J. Nabel, Flow cytometry reveals that H5N1 vaccination elicits cross-reactive stem-directed antibodies from multiple Ig heavy-chain lineages. *J. Virol.* **88**, 4047–4057 (2014).
55. J. E. Ledgerwood, C. J. Wei, Z. Hu, I. J. Gordon, M. E. Enama, C. S. Hendel, P. M. McTamney, M. B. Pearce, H. M. Yassine, J. C. Boyington, R. Bailer, T. M. Tumpey, R. A. Koup, J. R. Mascola, G. J. Nabel, B. S. Graham; VRC 306 Study Team, DNA priming and influenza vaccine immunogenicity: Two phase 1 open label randomised clinical trials. *Lancet Infect. Dis.* **11**, 916–924 (2011).
56. A. T. Widge, A. R. Hofstetter, K. V. Houser, S. F. Awan, G. L. Chen, M. C. B. Florez, N. M. Berkowitz, F. Mendoza, C. S. Hendel, L. A. Holman, I. J. Gordon, P. Apte, C. J. Liang, M. R. Gaudinski, E. E. Coates, L. Strom, D. Wycuff, S. Vasquez, J. Stein, J. G. Gall, W. C. Adams, K. Carlton, R. A. Gillespie, A. Creanga, M. C. Crank, S. F. Andrews, M. Castro, L. A. Serebryannyy, S. R. Narpala, C. Hatcher, B. C. Lin, S. O'Connell, A. W. Freyn, V. C. Rosado, R. Nachbagauer, P. Palese, M. Kanekiyo, A. B. McDermott, R. A. Koup, L. K. Dropulic, B. S. Graham, J. R. Mascola, J. E. Ledgerwood; VRC 321 study team, An influenza hemagglutinin stem nanoparticle vaccine induces cross-group 1 neutralizing antibodies in healthy adults. *Sci. Transl. Med.* **15**, ade4790 (2023).
57. T. Tiller, E. Meffre, S. Yurasov, M. Tsuiji, M. C. Nussenzweig, H. Wardemann, Efficient generation of monoclonal antibodies from single human B cells by single cell RT-PCR and expression vector cloning. *J. Immunol. Methods* **329**, 112–124 (2008).
58. N. A. Doria-Rose, J. N. Bhiman, R. S. Roark, C. A. Schramm, J. Gorman, G. Y. Chuang, M. Pancera, E. M. Cale, M. J. Ernandes, M. K. Louder, M. Asokan, R. T. Bailer, A. Druz, I. R. Fraschilla, N. J. Garrett, M. Jarosinski, R. M. Lynch, K. McKee, S. O'Dell, A. Pegu, S. D. Schmidt, R. P. Staupe, M. S. Sutton, K. Wang, C. K. Wibmer, B. F. Haynes, S. Abdool-Karim, L. Shapiro, P. D. Kwong, P. L. Moore, L. Morris, J. R. Mascola, New member of the V1V2-directed CAP256-VRC26 lineage that shows increased breadth and exceptional potency. *J. Virol.* **90**, 76–91 (2016).
59. X. Brochet, M. P. Lefranc, V. Giudicelli, IMGT/V-QUEST: The highly customized and integrated system for IG and TR standardized V-J and V-D-J sequence analysis. *Nucleic Acids Res.* **36**, W503–W508 (2008).
60. N. T. Gupta, J. A. Vander Heiden, M. Uduman, D. Gadala-Maria, G. Yaari, S. H. Kleinstein, Change-O: A toolkit for analyzing large-scale B cell immunoglobulin repertoire sequencing data. *Bioinformatics* **31**, 3356–3358 (2015).
61. M. Krzywinski, J. Schein, I. Birol, J. Connors, R. Gascoyne, D. Horsman, S. J. Jones, M. A. Marra, Circos: An information aesthetic for comparative genomics. *Genome Res.* **19**, 1639–1645 (2009).
62. A. Creanga, R. A. Gillespie, B. Fisher, S. F. Andrews, J. Lederhofoer, C. Yap, L. Hatch, T. Stephens, Y. Tsybovsky, M. C. Crank, J. E. Ledgerwood, A. McDermott, J. R. Mascola, B. S. Graham, M. Kanekiyo, A comprehensive influenza reporter virus panel for high-throughput deep profiling of neutralizing antibodies. *Nat. Commun.* **12**, 1722 (2021).
63. P. S. Lee, X. Zhu, W. Yu, I. A. Wilson, Design and structure of an engineered disulfide-stabilized influenza virus hemagglutinin trimer. *J. Virol.* **89**, 7417–7420 (2015).
64. C. Suloway, J. Pulokas, D. Fellmann, A. Cheng, F. Guerra, J. Quispe, S. Stagg, C. S. Potter, B. Carragher, Automated molecular microscopy: The new Leginon system. *J. Struct. Biol.* **151**, 41–60 (2005).
65. N. R. Voss, C. K. Yoshioka, M. Radermacher, C. S. Potter, B. Carragher, DoG Picker and TiltPicker: Software tools to facilitate particle selection in single particle electron microscopy. *J. Struct. Biol.* **166**, 205–213 (2009).
66. G. C. Lander, S. M. Stagg, N. R. Voss, A. Cheng, D. Fellmann, J. Pulokas, C. Yoshioka, C. Irving, A. Mulder, P. W. Lau, D. Lyumkis, C. S. Potter, B. Carragher, Appion: An integrated, database-driven pipeline to facilitate EM image processing. *J. Struct. Biol.* **166**, 95–102 (2009).
67. S. Q. Zheng, E. Palovcak, J. P. Armache, K. A. Verba, Y. Cheng, D. A. Agard, MotionCor2: Anisotropic correction of beam-induced motion for improved cryo-electron microscopy. *Nat. Methods* **14**, 331–332 (2017).
68. A. Rohou, N. Grigorieff, CTFFIND4: Fast and accurate defocus estimation from electron micrographs. *J. Struct. Biol.* **192**, 216–221 (2015).
69. K. Zhang, Gctf: Real-time CTF determination and correction. *J. Struct. Biol.* **193**, 1–12 (2016).
70. S. H. Scheres, RELION: Implementation of a Bayesian approach to cryo-EM structure determination. *J. Struct. Biol.* **180**, 519–530 (2012).
71. A. Punjani, J. L. Rubinstein, D. J. Fleet, M. A. Brubaker, cryoSPARC: Algorithms for rapid unsupervised cryo-EM structure determination. *Nat. Methods* **14**, 290–296 (2017).
72. P. D. Adams, K. Gopal, R. W. Grosse-Kunstleve, L. W. Hung, T. R. Ioerger, A. J. McCoy, N. W. Moriarty, R. K. Pai, R. J. Read, T. D. Romo, J. C. Sacchettini, N. K. Sauter, L. C. Storoni, T. C. Terwilliger, Recent developments in the PHENIX software for automated crystallographic structure determination. *J. Synchrotron Radiat.* **11**, 53–55 (2004).
73. T. C. Terwilliger, S. J. Ludtke, R. J. Read, P. D. Adams, P. V. Afonine, Improvement of cryo-EM maps by density modification. *Nat. Methods* **17**, 923–927 (2020).
74. P. Emsley, K. Cowtan, Coot: Model-building tools for molecular graphics. *Acta Crystallogr. D Biol. Crystallogr.* **60**, 2126–2132 (2004).
75. I. W. Davis, L. W. Murray, J. S. Richardson, D. C. Richardson, MOLPROBITY: Structure validation and all-atom contact analysis for nucleic acids and their complexes. *Nucleic Acids Res.* **32**, W615–W619 (2004).
76. B. A. Barad, N. Echols, R. Y. Wang, Y. Cheng, F. DiMaio, P. D. Adams, J. S. Fraser, EMRinger: Side chain-directed model and map validation for 3D cryo-electron microscopy. *Nat. Methods* **12**, 943–946 (2015).
77. E. F. Pettersen, T. D. Goddard, C. C. Huang, E. C. Meng, G. S. Couch, T. I. Croll, J. H. Morris, T. E. Ferrin, UCSF ChimeraX: Structure visualization for researchers, educators, and developers. *Protein Sci.* **30**, 70–82 (2021).

Acknowledgments: We thank D. Ambrozak for help with flow cytometry sorting and A. Ransier and F. Laboune for next-generation sequencing. **Funding:** This study was supported by the Intramural Research Program of the Vaccine Research Center and the Division of Intramural Research, National Institute of Allergy and Infectious Diseases, NIH (all authors); Simons Foundation grant SF349247 (to J.G.); and NIH National Institute of General Medical Sciences grant GM103310 (to J.G.). **Author contributions:** S.F.A. developed the study hypothesis, planned the experiments, developed methodology, performed flow cytometry and Ig sequencing, analyzed data, created the manuscript figures, and wrote the paper. L.Y.C., G.D.S., and J.E.R. performed flow cytometry and Ig sequencing, produced mAbs, and tested both mAbs and sera for binding. J.G., C.S.F.C., T.Z., D.R.H., and P.D.K. performed and supervised protein structure analysis. R.A.G. and A.C. performed serum and mAb neutralization assays. S.N. and L.Y.C. developed serum competition assays. J.B. and S.R.G. analyzed 10X Genomics data. I.G., L.H., and F.M. enrolled and monitored vaccine trial participants. G.L.C. and A.W. monitored safety and managed the clinical trial design and implementation. K.V.H. contributed to vaccine trial design and sample management. L.K.D. and J.E.L. provided oversight over all clinical activities. B.S.G., J.R.M., P.D.K., M.K., and A.B.M. provided study guidance and edited the manuscript. **Competing interests:** B.S.G., J.R.M., M.K., and P.D.K. are named inventors of U.S. patents 9,441,019, 10,137,190, and 10,363,301 on influenza hemagglutinin nanoparticle vaccines and stabilized hemagglutinin stem trimers filed by the Department of Health and Human Services (NIH). **Data and materials availability:** All data associated with this study are present in the paper or the Supplementary Materials. The cryo-EM map and fitted coordinates have been deposited to the Electron Microscopy Data Bank (EMDB) with accession code EMD-27139 and to the Protein Data Bank (PDB) with ID 8D21. Immunoglobulin sequences for mAbs were deposited in GenBank with accession numbers OP892531 to OP892750. Bulk sequencing reads were deposited in the NCBI Sequence Read Archive with BioSample accession numbers SAMN32398685 to SAMN32398691. Processed immunoglobulin sequences from bulk and single-cell sequencing are available at 10.6084/m9.figshare.21764174.

Submitted 19 August 2022
Accepted 10 January 2023
Published 19 April 2023
10.1126/scitranslmed.ade4976

Science Translational Medicine

An influenza H1 hemagglutinin stem-only immunogen elicits a broadly cross-reactive B cell response in humans

Sarah F. Andrews, Lauren Y. Cominsky, Geoffrey D. Shimberg, Rebecca A. Gillespie, Jason Gorman, Julie E. Raab, Joshua Brand, Adrian Creanga, Suprabhath R. Gajjala, Sandeep Narpala, Crystal S.F. Cheung, Darcy R. Harris, Tongqing Zhou, Ingelise Gordon, LaSonji Holman, Floreliz Mendoza, Katherine V. Houser, Grace L. Chen, John R. Mascola, Barney S. Graham, Peter D. Kwong, Alicia Widge, Lesia K. Dropulic, Julie E. Ledgerwood, Masaru Kanekiyo, and Adrian B. McDermott

Sci. Transl. Med., **15** (692), eade4976.
DOI: 10.1126/scitranslmed.ade4976

Science Translational Medicine (ISSN) is published by the American Association for the Advancement of Science. 1200 New York Avenue NW, Washington, DC 20005. The title *Science Translational Medicine* is a registered trademark of AAAS.